Pharmacological LXR activation with TO901317 modulates the expression profile of tumor-associated macrophages and the abundance of regulatory T cells in the tumor microenvironment

Jose M. Carbó[1,2*], Theresa E. León[1,3*], Joan Font-Díaz[1,4*], Juan Vladimir De la Rosa[5], Antonio Castrillo[5,6], Felix R. Picard[7], Daniel Staudenraus[7], Magdalena Huber[7], Lídia Cedó[8,9], Joan Carles Escolà-Gil[8,9], Lucía Campos[7,10], Latifa Bakiri[11], Erwin F. Wagner[11,12], Carme Caelles[4,13], Thomas Stratmann[1], Jo A. Van Ginderachter[14,15], Annabel F. Valledor[1,4]

[1]Department of Cell Biology, Physiology and Immunology, School of Biology, University of Barcelona, Barcelona, 08028 Spain.

[2]Leukaemia Stem Cell Group, Josep Carreras Leukemia Research Institute, Badalona, Spain.

[3]Department of Haematology, UCL Cancer Institute, University College London, UK.

[4]Institute of Biomedicine of the University of Barcelona (IBUB), Barcelona, Spain.

[5]Unidad de Biomedicina (Unidad Asociada al CSIC), Instituto Universitario de Investigaciones Biomédicas y Sanitarias (IUIBS), Grupo de Investigación Medio Ambiente y Salud (GIMAS, ULPGC). Universidad de Las Palmas de Gran Canaria, Las Palmas, Spain.

[6]Instituto de Investigaciones Biomédicas "Alberto Sols" CSIC-Universidad Autónoma de Madrid, Spain.

[7]Institute for Medical Microbiology and Hospital Hygiene, University of Marburg, Marburg, Germany.

[8]Institut d'Investigacions Biomèdiques (IIB) Sant Pau, Barcelona, Spain.

[9]CIBER de Diabetes y Enfermedades Metabólicas Asociadas, CIBERDEM, Hospitalet de Llobregat, Spain

[10]Departments of Gastroenterology and Hepatology, Erasmus MC-University Medical Center, Rotterdam, The Netherlands.

[11]Department of Laboratory Medicine, Medical University of Vienna, Austria.

[12]Department of Dermatology, Medical University of Vienna, Austria.

[13]Department of Biochemistry and Physiology, School of Pharmacy and Food Sciences, University of Barcelona, Barcelona, Spain.

[14]Lab of Cellular and Molecular Immunology, Vrije Universiteit Brussel, Brussels, Belgium.

[15]Lab of Myeloid Cell Immunology, VIB Center for Inflammation Research, Brussels, Belgium.

*Equal contributors.

Corresponding author: Dr. Annabel F. Valledor, Phone: +34-93-4039384; FAX: +34-93-4110358; e-mail address: afernandezvalledor@ub.edu

Running title: Pharmacological LXR activation modulates TAM gene expression

Keywords: Tumor-associated macrophages, IL-4, GM-CSF, LXR, Ccl17.

Conflict of Interest Statement: The authors declare no potential conflicts of interest.

Abstract

Liver X receptors (LXRs) are transcription factors from the nuclear receptor family that are activated by oxysterols and synthetic high-affinity agonists. In tumor progression studies using syngeneic Lewis Lung carcinoma, the synthetic LXR agonist TO901317 inhibited tumor growth in *wild-type* but not in LXR-deficient mice, indicating that the anti-tumor effects of the agonist depends on functional LXR activity in host cells. Pharmacological activation of the LXR pathway reduced the intratumoral abundance of regulatory T cells (Tregs) and the expression of the Treg attracting chemokine *Ccl17* by MHCII^{high} tumor-associated macrophages (TAM)s. Moreover, gene expression profiling indicated a broad negative impact of the LXR agonist on other mechanisms used by TAMs for the maintenance of an immunosuppressive environment. In studies exploring the macrophage response to GM-CSF or IL-4, the repression of IRF4 expression emerged as a mechanism used by activated LXRs to down-regulate IRF4-dependent genes, including *Ccl17*. Taken together, this work reveals combined actions of the LXR pathway in the control of TAM responses that contribute to the anti-tumoral effects of pharmacological LXR activation and provides new insights for the development of novel therapeutic options for the treatment of cancer.

Statement of Significance: This work reveals unrecognized roles of LXRs in the transcriptional control of the tumor microenvironment, which may help design novel therapeutic options for the treatment of cancer.

Introduction

Nuclear receptors are a family of transcription factors with key functions in health and disease. Many members within this family are activated in a ligand-dependent manner. In particular, liver X receptors (LXRs) are activated by cholesterol derivatives, including specific oxysterols, and by synthetic high-affinity agonists. Two LXR subtypes have been identified, LXRα (NR1H3) and LXRβ (NR1H2), which are expressed in tissues in an overlapping but not identical manner. Both LXRs bind to DNA as heterodimers with another subgroup of the nuclear receptor family, the retinoid X receptors (RXRs), to regulate positively the transcription of a variety of target genes involved in lipid and glucose metabolism (revised in (1)) and in immune cell function (2–6). Moreover, upon ligand-binding, LXRs repress inflammatory gene expression (revised in (7)).

Synthetic LXR agonists activate different mechanisms that translate into anti-proliferative effects in a wide variety of cancer cell types (revised in (8)). *In vivo* studies, however, have produced contradictory results on the role of the LXR pathway in controlling tumor growth. In several mouse models of cancer, LXR agonists efficiently reduced primary tumor growth (9–11). Interestingly, while inhibiting the metastasis of melanoma cells in an apolipoprotein E (ApoE)-dependent manner (9), the agonist GW3965 exacerbated the dissemination of breast cancer cells to the lung (10). Another study showed that endogenous LXR ligands can be secreted by tumor cells as a strategy for immune evasion (12). In that setting, the activation of LXRα repressed the expression of CC chemokine receptor (CCR)7 on dendritic cells, thus impairing their migration to lymphoid organs and compromising the establishment of an anti-tumor adaptive immune response. Conversely, recent work has shown that LXR agonism, and

subsequent APOE production, reduces the levels of myeloid-derived suppressor cells (MDSCs), thus enhancing CTL activity (11). These contrasting observations support the need to dissect the roles of the LXR pathway in the tumor microenvironment in different contexts of cancer.

Solid tumors are infiltrated by heterogeneous populations of leukocytes. Among the immune cells within the tumor site, tumor-associated macrophages (TAMs) are particularly abundant and present at all stages of tumor progression. Interestingly, TAMs have been associated with poor prognosis in a variety of cancers (13,14). In most solid tumors, TAMs exhibit pro-tumoral functions by promoting cancer cell survival and proliferation, extracellular matrix remodeling and angiogenesis that benefit tumor cell migration and dissemination to secondary locations (15). TAMs also adopt immune suppressive roles within the tumor microenvironment. Through the surface expression of a number of regulatory molecules, TAMs are able to directly suppress immune responses against tumor cells. For instance, TAMs express human leucocyte antigen (HLA)-C, HLA-G and HLA-E which inhibit the activation of NK cells, and ligands for programmed cell death protein 1 (PD-1) or CTL antigen 4 (CTLA4) (PD-L1 and B7-1, respectively), which inhibit T cell proliferation and activation, as well as the cytolytic activity of $CD8^+$ T cells. TAMs can also influence the anti-tumoral immune response indirectly through the induction of L-arginine consuming enzymes, namely nitric oxide synthase (NOS)2 and arginase 1, and the secretion of an array of cytokines and chemokines (revised in (16)). For example, TAMs secrete CC chemokine ligand (Ccl)17 and Ccl22 upon stimulation by granulocyte/monocyte-colony stimulating factor (GM-CSF) produced by tumor cells (17,18). Through their binding to surface CCR4, Ccl17 and Ccl22 promote the migration of regulatory T cells (Tregs) to the tumor

microenvironment (19,20), thus facilitating the establishment of an immunosuppressive environment.

In mice, different TAM populations have been identified within solid tumors, displaying markers that partially fit with the classical *versus* alternative macrophage activation paradigm (21). TAMs exhibiting a more pro-inflammatory gene signature are enriched in normoxic areas of the tumor and express high levels of MHCII, whereas TAMs displaying a more alternative phenotype are located mostly within hypoxic tumor areas, have a superior pro-angiogenic activity and express low MHCII levels (22). Nevertheless, both TAM subsets are poor antigen presenting cells, express Ccl17 and Ccl22 (although $MHCII^{high}$ TAMs produce higher levels of these chemokines) and are able to suppress T-cell activation.

In this work we demonstrate unrecognized roles of LXRs in the control of TAM gene expression. The synthetic LXR agonist TO901317 (T1317) inhibited the growth of syngeneic Lewis Lung carcinoma in *wild-type* (WT) but not in LXR-deficient ($LXR\alpha/\beta^{-/-}$) mice, despite the fact that injected cancer cells express LXR isoforms in both settings and that these cells are sensitive to growth inhibition by high doses of LXR agonists *in vitro*. This indicates that LXR activity in host cells is essential for the anti-tumor effects of the synthetic LXR agonist. In this context, several mechanisms used by TAMs for the maintenance of an immunosuppressive environment were down-regulated upon pharmacological LXR activation, including the expression of the chemokine CCL17, which correlated with a decrease in the abundance of intratumoral Tregs *in vivo*. In addition, LXR activity repressed other genes that are part of the pro-tumoral program of TAMs and reduced partially the capability of these cells to suppress T cell proliferation *in vitro*. Moreover, repression of IRF4 expression emerged as a mechanism linking

LXR activation with the down-regulation of selective genes, such as *Ccl17*, in different macrophage populations. Taken together, this work provides novel insights about the biological actions of LXR agonists and supports their pharmacological use as anti-tumoral drugs.

Materials and Methods

Reagents. The synthetic high affinity LXR agonists T1317 and GW3965 were purchased from Cayman Europe and Tocris, respectively. Recombinant murine GM-CSF and interleukin (IL)-4 and human IL-4 and macrophage-colony stimulating factor (M-CSF) were purchased from PeproTech.

Animals. C57BL/6 mice were purchased from Harlan and raised as a colony in our animal facility. LXR-deficient mice were initially donated by Dr. David Mangelsdorf (UT Southwestern Medical Center, Dallas, TX, USA) and backcrossed into C57BL/6 background for more than ten generations. Foxp3EGFP mice were generated by crossing the NOD.Foxp3EGFP strain (23) with C57BL/6 mice for five generations. PyMT mice (24) with an FVB/N background were obtained from The Mouse Models of Human Cancers Consortium Repository (National Cancer Institute, Frederick, MD, USA) and backcrossed into the C57BL/6 background for nine generations. Three week-old JunB f/f; MxCre mice (25) and Cre-negative control littermates (C57BL/6 background) were administered three intra-peritoneal injections of poly I:C at weekly intervals to induce JunB deletion systemically (including the hematopoietic lineage/bone marrow). JunD-deficient mice (26) and WT control littermates were generated by heterozygote intercrosses (C57BL/6 background). IRF4-deficient mice and control C57BL/6 mice were bred at the animal facility of the Biomedical Research Center at the University of Marburg, Germany. Unless otherwise stated, the mice were fed a regular chow diet. All the protocols requiring animal manipulation have been approved by the Institutional Animal Care and Use Committees from Parc Científic de Barcelona (#9672), Universitat de Barcelona (#7088), Institut de Recerca de l'Hospital

de la Santa Creu i Sant Pau (#7281) and the University of Marburg (RP Giessen, Germany).

Cells. Bone marrow-derived macrophages were obtained from six to ten-week-old mice as described (27). Bone marrow precursors were differentiated to macrophages in DMEM supplemented with 20% heat inactivated FBS (Sigma-Aldrich) and 30% L929 conditioned media as a source of M-CSF.

Human macrophages were differentiated *in vitro* from peripheral blood mononuclear cells (PBMCs) from healthy donors. See more details in Supplemental Methods. The protocol has been approved by the Bioethics Commission of the University of Barcelona and the blood samples were obtained from the Blood and Tissue Bank from *Generalitat de Catalunya*.

The 3LL-R cell line (28) was maintained in RPMI media with L-glutamine (L-Gln, 0.3 g/L) (BioWest) supplemented with 10% FBS. Raw264.7 macrophages (ATCC, RRID: CVCL_0493) were cultured in DMEM-10% FBS. All cell lines were used within 15 passages after thawing.

Tumor progression studies. 3LL-R cells ($3x10^6$) were subcutaneously injected in eight to ten-week-old WT or LXRα/β-deficient male mice. The tumors were allowed to grow for two weeks. From day 7 to day 15, length (D) and width (d) measures were taken with a digital caliper and tumor volume was calculated using the formula $V = \pi$ x (d2 x D)/6 (29). In some experiments, at day 7, once the tumor was established and for the next 8 days, the animals received a daily dose of T1317 (15 mg/kg) through an intra-peritoneal injection. Control animals received an equivalent dose of vehicle (DMSO)

diluted in PBS. At day 15, the mice were euthanized and the tumors excised and processed.

Alternatively, tumor development was evaluated in PyMT transgenic mice. After weaning, PyMT female mice were administered either a regular chow diet (A04; Scientific Animal Food & Engineering) or the same diet supplemented with 50 mg/kg of T1317. The mice were monitored every three days for palpable tumors starting at six weeks of age. Tumor latency was defined as the time to the development of the first palpable tumor in each mouse. The mice were euthanized at 22 weeks of age. Total tumor burden was determined after all the mammary glands were excised and weighed, and the mass of the tumor-bearing mammary glands was measured. Each mammary gland was numerically labelled as in (30).

Identification of immune cell populations. 3LL-R cells ($3x10^6$) were injected subcutaneously in recipient mice as described above. At day 15 post-injection, the tumors were dissected and processed as indicated in Supplemental Methods. The final cell suspension was diluted to a concentration of 10^7 cells/ml in PBS and incubated first with Fc block (rat anti-mouse CD16/CD32, BD Biosciences) (1:50 dilution, 30 min, 4^oC). For myeloid cell determination, the cells were incubated with specific antibodies against CD11b, Ly6G, Ly6C and IA/IE (MHCII) (See more details in Supplemental Methods) (21). Cell populations were analyzed through flow cytometry using a FACSaria Fusion cell sorter (BD Bioscience) (see gating strategy in Supplemental Figure S1).

For lymphoid cell determination, the cells were incubated with specific antibodies against CD4 and CD8 (See more details in Supplemental Methods and Supplemental

Figure S1) The cells were then permeabilized and fixed using the Foxp3/Transcription factor staining buffer set (Invitrogen) following the manufacturer's specifications. The cells were analyzed by flow cytometry.

Alternatively, for lymphocyte cell determination, 3LL-R cells were injected subcutaneously in Foxp3EGFP reporter mice. The tumors were collected at day 10 post-cancer cell injection. Cell suspensions were blocked with Fc block and incubated with specific antibodies against CD4 and CD8 (Supplemental Methods). The cells were analyzed by flow cytometry. Tregs were identified via EGFP expression analysis (Supplemental Figure S1).

In some experiments, the spleens were also harvested. See details in Supplemental Methods. Lymphocyte populations were analyzed as described above.

Treg depletion. To downregulate the frequency of Tregs within tumors, male Foxp3EGFP reporter mice were administered antibodies anti-CD25 (InVivoMab anti-mouse CD25 (IL-2Ra), clone PC-61.5.3, Bio X Cell (#BE0012)) (200 μg per animal diluted in PBS; intra-peritoneal injection) at days 2, 5 and 8 post-tumor cell injection. Control mice were administered the isotype control (InVivoMAb rat IgG isotype control anti-horseradish peroxidase, clone HRPN, Bio X Cell (#BE0088)). At day 5, and until day 9, the mice received a daily dose of T1317 (15 mg/kg) or vehicle (DMSO) through intra-peritoneal injection. From day 5 to day 10, tumor progression was evaluated. At day 10, the mice were euthanized, and the spleens and tumors were recovered and processed as described above.

Isolation of TAMs. 3LL-R cells were injected subcutaneously in recipient C57BL/6 mice and, at day 15 post-injection, the tumors were excised and processed as described above. Cells suspensions were generated from pooled tumors (five tumors per sample) and incubated with the antibodies described for myeloid cell determination. $MHCII^{low}$ TAM and $MHCII^{high}$ TAM populations were isolated using a FACSaria Fusion cell sorter (BD Bioscience). For *ex vivo* experiments, TAMs were cultured in RPMI-10% FBS, supplemented with L-glutamine, HEPES, 10 mM sodium pyruvate, non-essential amino acids (BioWest) and 3.7 nM 2-mercaptoethanol (Sigma-Aldrich).

Isolation of Tregs. 3LL-R cells were injected subcutaneously in Foxp3EGFP transgenic mice. At day 10 post-injection, cell suspensions were generated from pooled tumors and Tregs were sorted as $EGFP^{+}$ cells using a FACSaria Fusion cell sorter. The cells were maintained in RPMI-10% FBS for subsequent analysis. Alternatively, Tregs were isolated from the spleens of Foxp3EGFP mice.

Proliferation Assays. 3LL-R cells were plated in 24-well plates (10^5 cells/well) and starved in RPMI without FBS during 24 h in the presence of LXR ligands or vehicle (DMSO). After starvation, the cells were incubated with 10% FBS and 0.3 g/L L-glutamine for 24 h. Finally, the cells were pulsed with ^{3}H-thymidine (1 μCi/ml; ICN Pharmaceuticals) for 6 h. The cells were fixed in 70% methanol, washed in 10% TCA and lysed in 1% SDS/0.3 M NaOH. Radioactivity was counted by liquid scintillation using a 1400 Tri-Carb Packard counter (GMI). Each experimental condition was performed in triplicates.

Purified Tregs (10^5 cells/well) were stained with CellTrace CFSE cell proliferation kit (Invitrogen) following the manufacturer's recommendations and then stimulated with T1317 (1 μM) or DMSO for 18 h at 37 ºC. Unstained cells were grown separately as a negative control for cytometry. Treg proliferation was induced during 48 h using the mouse T cell activation/expansion kit (Miltenyi Biotec), which consists of anti-biotin MACSiBead™ particles and biotinylated antibodies against mouse CD3ε and CD28, in the presence of IL-2 (100 U/ml). Cell proliferation was analyzed by flow cytometry as the percentage of cells with CFSE dispersion compared to non-activated Tregs. Murine IL-2 was expressed in and purified from E. coli as described (31).

Suppression of T cell proliferation. TAMs or Tregs were seeded in 96 well plates (200,000 TAMs/well or 100,000 Tregs/well in RPMI-10% FBS) and stimulated with T1317 (1 μM) or DMSO for 18 h at 37 ºC. In experiments using TAMs, the medium was then replaced by fresh medium (without LXR agonist). Total splenocytes were obtained from the spleens of C57BL/6 mice as a cell suspension and stained with the CellTrace CFSE cell proliferation kit. Unstained splenocytes were grown separately as a negative control for cytometry. CFSE-stained splenocytes were either grown alone in RPMI-10% FBS or incubated with TAMs or Treg cells at a 1:1 ratio. T cell proliferation was induced using the mouse T cell activation/expansion kit during 48 h at 37ºC and analyzed by flow cytometry.

Phagocytosis assay. $MHCII^{low}$ TAMs and $MHCII^{high}$ TAMs were seeded in 24 well plates (500,000 cells/well) and stimulated with T1317 1 μM or DMSO for 18 h at 37 ºC. The cells were incubated with 3 μm fluorescent microspheres (Fluoresbrite YG

microspheres, Polysciences) at a ratio of 20 beads/cell for 30 min at 37 ºC. After this time, the cells were placed on ice, washed three times with ice-cold PBS, and fixed in PBS-2% PFA. The phagocytosis of microspheres was analyzed by flow cytometry.

RNA extraction, cDNA synthesis and quantitative real-time PCR analysis. Total RNA was extracted from cells or tissues using Trizol (Invitrogen) as recommended by the manufacturer. For cDNA synthesis, 1μg of RNA was subjected to reverse transcription using M-MLV Reverse transcriptase RNase H Minus, Point Mutant, oligo$(dT)_{15}$ primer and PCR nucleotide mix (Promega). Quantitative real time PCR (qPCR) was performed using the Power SYBR Green Reagent Kit (Applied Biosystems) following the manufacturer's recommendations. See more details in Supplemental Methods. The data were expressed as mRNA levels relative to ribosomal *L14* or to *Gapdh* expression in murine and human samples, respectively.

Gene expression profiling. Total RNA was purified using the RNAeasy Kit (Qiagen) following the manufacturer's instructions. The samples were processed as described in Supplemental Methods and hybridized to GeneChip Mouse Clariom S Array (Affymetrix). For each sample, expression estimates were calculated from probe intensities and represented as log2 values. Heat maps were produced with Heatmapper (Wishart Research Group, University of Alberta, Canada). Gene ontology (GO) analysis was carried out with the PANTHER Classification System (32). Microarray data have been deposited at the ArrayExpress database with accession number E-MTAB-9707.

Identification and cloning of potential enhancer regions with IRF4 binding sites. Public data from ChIP-seq experiments (GSE40918) (33) were mapped with Bowtie2 to the mm9 assembly of the mouse genome. The resulting SAM files were subsequently analyzed using HOMER. Each sequencing experiment was normalized to 107 uniquely mapped tags. Sequencing experiments were visualized at UCSC genome browser from tracks generated with HOMER. IRF4 binding sites were identified and annotated using HOMER. Regions of interest showing IRF4 peaks were scanned for IRF4 binding motifs using public JASPAR motif matrix with DMINDA (34).

Potential enhancer regions containing IRF4 binding sites upstream and downstream of the Ccl17 gene were amplified from mouse tail genomic DNA using REDExtract N-Amp PCR Ready Mix (Sigma-Aldrich). See more details in Supplemental Methods. Amplified regions were subsequently cloned between the KpnI and XhoI restriction sites of a pGL3-promoter vector (Promega).

Reporter activity assays. To evaluate the potential activity of Ccl17 enhancers containing IRF4 binding sites, Raw264.7 macrophages (10^5 cells/well in 12-well plates) were co-transfected with 100 ng of the enhancer-containing pGL3 plasmid and either 100 ng of a pMIG-IRF4 plasmid that constitutively expresses IRF4 (gift from David Baltimore, California Institute of Technology, Pasadena, CA, USA; Addgene plasmid # 58987) (35) or an empty vector. All cells were co-transfected with 500 ng of pCDNA3-LXRα plasmid that constitutively expresses LXRα to ensure an optimal response to LXR ligands and 10 ng of a renilla expression plasmid (pBOS-Renilla) as a control of the transfection efficiency. Transfections were carried out using Superfect (Qiagen)

following the manufacturer's instructions. Luciferase activity was assessed using the Dual Luciferase Reporter Assay (Promega) in an Infinite M200 luminometer (Tecan).

Protein extraction and western blot analysis. The cells were washed twice in cold PBS and lysed on ice with lysis solution (1% Triton X-100, 10% glycerol, 50 mM HEPES, pH 7.5, 250 mM NaCl, protease inhibitors, 1 mM sodium orthovanadate). Insoluble material was removed by centrifugation at 13,000 x g for 8 min at 4°C. Cell lysates were processed for western blot analysis as described in Supplemental Methods.

ELISA. The supernatants from macrophage cultures were recovered and stored at -80 ^{o}C. ELISA kits from Thermo Scientific (Mouse MDC (CCL22) ELISA kit and Mouse TARC (CCL17) ELISA kit) were used for quantitative measurement of secreted mouse CCL22 and CCL17, respectively, using the manufacturer's recommendations. See a more detailed protocol in Supplemental Methods.

Statistical Analysis. The GraphPad Prism 6.0 software was used to perform all statistical analyses. Differences in tumor volume in the 3LL-R model were analyzed by a two-way repeated-measure ANOVA with a Bonferroni *post hoc* test. The log-rank and Gehan-Wilcoxon tests were used to compare tumor latency curves in the PyMT model. The rest of the data was analyzed using either one way ANOVA, or two-tailed Student's *t*-test for data with normal distribution, or the non-parametric Kruskal Wallis-Dunn's test or Mann–Whitney U test for data not following normal distribution.

To make different experiments comparable in Figures 4C, 5A-D and F, 6A-C, and 7C-E, and K, and Supplemental Figures S2C-D and S5, the data were normalized using the following procedure. The intensity of each experiment (ie) was calculated by determining the mean value of gene expression between the negative and positive controls. The intensities of separate experiments were normalized by the mean intensity value of all the experiments (im) and, for each experiment, the resulting normalization factor (im/ie) was multiplied by the expression levels of all the samples in that experiment. In Figures 2A-B, the data was normalized using the mean percentage of cells in the DMSO group in each experiment.

Results

Functional LXR expression in host cells is required for the anti-tumoral actions of the LXR agonist T1317

We and others had previously reported anti-proliferative actions of LXR agonists in primary immune cells (36,37) and in tumor cell lines *in vitro* (revised in (8)). These observations were confirmed in this study using the Lewis lung carcinoma cell line 3LL-R, which expresses both LXRα and β (Figures 1A and 1B). Interestingly, however, tumor progression studies based on the subcutaneous injection of 3LL-R cells into syngeneic mice (C57BL/6 background) revealed that the administration of the LXR agonist T1317 was able to inhibit the growth of established tumors in WT mice, but not in mice lacking functional LXRs (Figures 1C and 1D) despite the fact that the injected cancer cells express LXRs. Altogether, these observations suggest that LXR expression in host cells is essential for the inhibitory actions of the synthetic LXR agonist on tumor growth.

The LXR agonist was also effective in preventing tumor growth in PyMT female mice, a model for spontaneous breast adenocarcinoma development and progression (Figure 1E-G). The oral administration of the agonist through the diet did not affect tumor latency (Figure 1E), but resulted in a significant decrease in mammary gland weight at 22 weeks of age (Figures 1F and 1G). This finding argues for the importance of LXR activity in the microenvironment once tumors are established, rather than affecting cancer cell proliferation and early-stage carcinogenesis.

Pharmacological LXR activation reduces the abundance of Tregs within the tumor

In order to dissect the actions of the LXR agonist in the tumor microenvironment, we next used flow cytometry to assess, in 3LL-R tumors, the abundance of different intratumoral immune cell populations that have prognostic values. At the level of myeloid cells, several populations were distinguished in 3LL-R tumors: $CD11b^{+}/Ly6C^{high}/Ly6G^{-}$ cells (compatible with $Ly6C^{high}$ monocytes and monocytic MDSCs), $CD11b^{+}/Ly6C^{low}/Ly6G^{+}$ cells (compatible with neutrophils and polymorphonuclear MDSCs), tumor-associated dendritic cells (TADCs) ($CD11b^{+}/Ly6C^{-}/Ly6G^{-}/MHCII^{bright}$), and two TAM subsets ($CD11b^{+}/Ly6C^{-}/Ly6G^{-}$) expressing different levels of MHCII and termed $MHCII^{low}$ TAMs and $MHCII^{high}$ TAMs (gating strategy shown in Supplemental Figure S1). Pharmacological LXR activation specifically decreased the frequency of $MHCII^{high}$ TAMs without significantly affecting the frequency of other myeloid cell populations analyzed here (Figure 2A). However, the total numbers of $MHCII^{high}$ TAMs differed considerably between tumors and only a tendency toward a decreased amount of these cells (when normalized to the weight or volume of the tumor) was observed in the tumors from T1317-treated WT mice (Figure 2F). These observations suggest that the decrease in the relative frequency of $MHCII^{high}$ TAMs in response to LXR activation does not consistently reflect reduced absolute numbers of these cells in the tumor.

At the level of T lymphocytes, the administration of T1317 significantly decreased the frequency and the total numbers of $CD4^{+}Foxp3^{+}$ Tregs within the tumor (Figures 2B-D). In addition, decreased levels of *Foxp3* expression were observed in the mammary glands from T1317-treated PyMT mice in comparison with mice fed a regular diet (Figure 2E), which suggests that T1317 may also downregulate Treg infiltration in spontaneous breast adenocarcinoma. In LXR-deficient mice, T1317 did not inhibit the total numbers of the immune cell populations tested, including Tregs (Figure 2F), which

is in line with the LXR-specific effects of the agonist in the control of tumor growth (Figure 1C-D).

Since a major goal of this study was to characterize the mechanisms underlying the anti-tumoral actions of synthetic LXR agonists, we further explored the effects of LXR activation in Tregs. First, the treatment of tumor-bearing mice with T1317 did not impact the frequency of Tregs in the spleen (Figure 2G), suggesting that the decrease in Treg abundance is specific to the tumor. Of note, the frequency of splenic $CD4^+$ $Foxp3^-$ cells was down-regulated upon pharmacological LXR activation (Figure 2G), in line with previous work showing a role for LXR in the negative control of central T cell proliferation (36). Next, we evaluated whether the immunosuppressive capacity of Tregs is affected by T1317. Tregs were isolated from either the spleens or tumors of Foxp3EGFP reporter mice and treated with the LXR agonist or vehicle. Their capability to inhibit T cell proliferation induced by anti-CD3/CD28 antibodies was tested *in vitro*. Interestingly, the LXR agonist did not impair the suppressive capacity of Tregs on T cell proliferation (Figure 3A). Moreover, activation of LXRs did not reduce the expression of the anti-inflammatory cytokines *Il10* and *Tgfb* in Tregs from the spleen (Figure 3B). Taken together, these results suggest that pharmacological LXR activation does not inhibit the immunosuppressive capacity of the Treg itself, but rather results in a decrease in the amount of Tregs within the tumor. In addition, the LXR agonist did not inhibit the polyclonal proliferation of Tregs (Figure 3C).

Importantly, higher infiltration of Tregs often correlates with less favorable outcomes in different types of tumors and accumulated evidence indicates that the removal of Tregs is able to enhance anti-tumor immune responses (reviewed in (38)). To assess the relevance of the Treg population in the anti-tumoral actions of T1317, the levels of

Tregs were reduced by the intraperitoneal injection of monoclonal antibodies against CD25 in Foxp3EGFP reporter mice (Figure 3D). In comparison to control mice (injected with isotype control antibodies), Treg depletion resulted in reduced tumor progression (Figure 3E). In line with the data in Figures 2B-C, treatment with T1317 reduced the frequency of intratumoral Foxp3-GFP^{+} Tregs (Figure 3D) and inhibited tumor progression in control mice (Figure 3E). Interestingly, the LXR agonist was not effective in reducing tumor volumes in mice undergoing anti-CD25-mediated Treg depletion (Figure 3E), which suggests that the actions of T1317 in tumor progression are Treg-dependent.

Pharmacological LXR activation down-regulates *Ccl17* expression in TAMs

Treg abundance in the tumor has been shown to correlate with the local production of the chemokines CCL17 and CCL22 (19,20,39). Interestingly, TAMs, predominantly MHCII^{high} TAMs in mice, highly contribute to the secretion of these chemokines in the tumor microenvironment (21). Given our observations on Treg abundance, we next sought to investigate the impact of LXR activation on chemokine expression by TAMs from 3LL-R tumor-bearing mice. Interestingly, the treatment of WT mice with T1317 resulted in the reduced expression of *Ccl17* in MHCII^{high} TAMs, but not in TAMs from LXR-deficient mice (Figure 4A-B). Culturing these cells *in vitro* led to a drastic drop in *Ccl17* mRNA levels (compare Figures 4A and 4C), which suggests that the expression of this chemokine in MHCII^{high} TAMs is highly dependent on signals present in the tumor microenvironment. *Ex vivo* administration of the LXR agonist had little impact on *Ccl17* expression under these conditions (Figure 4C). A tendency for the down-regulation of *Ccl17* was also observed in MHCII^{low} TAMs from T1317-treated WT mice (Figure 4A). When WT MHCII^{low} TAMs were treated *ex vivo* with the LXR

agonist, clear inhibitory effects were observed on *Ccl17* and *Ccl22* expression (Figure 4C), suggesting that the production of such chemokines by this TAM population may also be susceptible to down-regulation by LXRs provided that the agonist can reach the (hypoxic) areas within the tumor where these cells reside.

We further explored whether the pharmacological activation of LXRs affects other pathways that may be involved in the maintenance of an immunosuppressed tumor microenvironment. Both $MHCII^{high}$ and $MHCII^{low}$ TAMs were isolated from established tumors and treated with the LXR agonist *ex vivo*. When incubated with splenocytes, both TAM subsets were able to suppress T cell proliferation (Figure 4D). Interestingly, the pre-treatment with the LXR agonist counteracted partially the suppressive capacity of TAMs. In contrast, their capability to phagocytose latex microspheres was not downregulated by the agonist (Figure 4E).

Microarray studies were performed in order to evaluate global effects on gene expression and some of the actions were validated in independent experiments through qPCR analysis (Figure 4F-G and Supplemental Figures S2, S3 and S4). The expression of the isoforms LXRα and LXRβ and of their heterodimeric partners RXRα and RXRβ was confirmed in both TAM subpopulations and stimulation with the LXR agonist did not change their expression levels (Supplemental Figure S2A), as is the case in many other cellular systems. Low levels of RXRγ were detected in these cells. As expected, several genes previously recognized as direct targets of the LXR-RXR heterodimer were induced in both TAM subsets (Supplemental Figure S2B). In contrast to observations in other cell types, however, no induction of *ApoE* expression was observed in TAMs treated with T1317 (Supplemental Figure S2B-C). Similar results

were obtained from whole tumors exposed to the LXR agonist *in vivo* (Supplemental Figure S2D).

We used the gene expression profiling data to further characterize the effects of the LXR agonist on selected markers of macrophage activation, including surface markers, enzymes, cytokines and chemokines other than Ccl17/Ccl22 (Supplemental Figure S3). As demonstrated in previous work (21), MHCII^{high} and MHCII^{low} TAMs differ in the levels of expression of a number of activation markers. The expression of most of the genes selected for this analysis was unaffected by the LXR agonist. However, significant downregulation was observed in the expression of several markers of activation (*Cd80, Nos2, Il1b, Il10, Il4ra, Mmp9* and *Ptges*) in T1317-treated MHCII^{high} TAMs.

In parallel, whole profiling analysis revealed that different subsets of genes were repressed (> 25 % repression) by T1317 in MHCII^{high} and MHCII^{low} TAMs (Supplemental Figure S4A). An unbiased GO analysis of genes repressed by T1317 in MHCII^{high} TAMs showed the enrichment of several biological processes, including the positive regulation of nitric oxide and reactive oxygen species (ROS) biosynthesis (Supplemental Figure S4B), which are important biological mechanisms contributing to the maintenance of an immunosuppressive state by tumor-infiltrated myeloid cells. No significant enrichment of specific biological processes was observed among the genes repressed by T1317 in MHCII^{low} TAMs. In addition, we selected a list of genes with reported involvement in immunosuppression in tumors and/or in the acquisition of a macrophage alternative activation phenotype. T1317 repressed the expression of several genes within this category in MHCII^{high} TAMs and MHCII^{low} TAMs (Figure 4F). The fact that the agonist was able to repress a larger set of genes in MHCII^{high} TAMs

(Figures 4F-G) suggests differences between both cell subpopulations in the repertoire of genes susceptible to LXR-mediated repression.

Synthetic LXR agonists inhibit the induction of *Ccl17* and *Ccl22* by IL-4 or GM-CSF

Ccl17 and *Ccl22* expression in cells from the monocyte-macrophage lineage is regulated by GM-CSF and IL-4 (40–42). Moreover, GM-CSF has been shown to induce *Ccl17* expression in MHCII^{high} TAMs *in vivo* (18). Considering the repressive effect of LXR agonism on *Ccl17* expression in TAMs, we further explored whether synthetic LXR agonists modulate the actions of GM-CSF or IL-4 in macrophages. In these experiments, bone marrow-derived macrophages, obtained from either WT or LXR$\alpha/\beta^{-/-}$ mice, were pre-incubated with the LXR agonists GW3965 or T1317 and then stimulated with IL-4 or GM-CSF for different periods of time. Pharmacological activation of the LXR pathway inhibited the expression of *Ccl17* and *Ccl22* induced by IL-4 (Figure 5A-B), whereas other key marker genes of the macrophage response to IL-4 were not affected (Figure 5A). The effects of the agonists on chemokine expression were drastically reduced or abolished in LXR-deficient macrophages (Figure 5C-D), indicating that these effects largely depend on functional LXR activity. In line with the changes in gene expression, pharmacological activation of LXRs inhibited the secretion of CCL17 and CCL22 in WT macrophages (Figure 5E). Interestingly, the induction of these chemokines at different time points after IL-4 treatment was significantly higher in LXR-deficient macrophages than in WT cells (Figure 5E-F), suggesting that LXRs can perform basal repression of these chemokines in the absence of synthetic high affinity agonists. Of note, the expression of LXRs was not reciprocally inhibited by IL-4

(Figure 5G) and the effects of the LXR agonist could not be attributed to changes in the pattern of STAT-6 phosphorylation in response to IL-4 (Figure 5H).

Stimulation with T1317 or GW3965 also resulted in lower production of *Ccl17* and *Ccl22* in response to GM-CSF (Figure 6A and D). Notably, and contrary to the effects on the IL-4 response, LXR agonists negatively impacted other GM-CSF target genes such as *Arg1*, *Retnla* and *Mgl2* (Figure 6A) and GM-CSF itself down-regulated *Lxra* expression (Figure 6B), suggesting a more general reciprocal negative interaction between GM-CSF signaling and the LXR pathway. Nevertheless, the effects of the agonists were abolished or severely reduced in LXR-deficient cells (Figure 6C-D).

Pharmacological LXR activation inhibits IRF4 expression

Despite the use of different signaling modules, macrophage responses to IL-4 and GM-CSF share the induction of the transcription factor IRF4 (41,43). The use of IRF4-deficient ($IRF4^{-/-}$) macrophages showed that the functional expression of IRF4 is required for the induction of a subset of the genes evaluated, namely *Ccl17*, *Ccl22*, *Retnla* and *Il1b*, but not for *Arg1*, *Mrc1* and *Mgl2* (Figure 7A-B). Of note, *Ccl17* and *Ccl22*, which are inhibited by LXR agonists during the macrophage response to both IL-4 and GM-CSF, were the most drastically impaired genes in $IRF4^{-/-}$ macrophages.

IRF4 has been shown to cooperatively bind activator protein-1 (AP1) complexes in T cells in order to regulate gene transcription from AP1-IRF composite elements (44). We therefore evaluated whether the induction of IRF4-dependent genes required cooperation with JunB or JunD. Although we cannot discard redundant roles from these proteins, the up-regulation of *Ccl17*, *Ccl22*, *Retnla* and *Il1b* in response to IL-4 or GM-

CSF was not impaired in macrophages deficient for either JunB or JunD (Supplemental Figure S5).

Interestingly, the expression of IRF4 itself during the macrophage response to IL-4 or GM-CSF was inhibited by LXR agonists both at the mRNA and protein level (Figure 7C-G). It has been recently reported that both cytokines induce the up-regulation of the expression of the demethylase jumonji domain-containing protein 3 (Jmjd3) upstream of the transcriptional activation of IRF4 (45,46). However, LXR activity did not repress the expression of this enzyme in response to IL-4 or GM-CSF (Supplemental Figure S6), which suggests that the inhibitory effects on IRF4 expression reported here are not related to upstream alterations in Jmjd3.

Previous work had analyzed the binding of IRF4 across the murine genome in T cells through ChiP-Seq analysis (33). By reanalyzing these data, we identified three sites with enriched binding of IRF4 in the proximity of the *Ccl17* gene both in naïve $CD4^+$ T cells and during Th17 cell differentiation (Supplemental Figure S7). To translate this finding to macrophages, we transfected Raw264.7 cells with reporter plasmids containing various IRF4 binding regions. Peak 2, located approximately 6.5 Kb upstream of the *Ccl17* transcription start site, displayed strong enhancer activity in response to IL-4, which was down-regulated upon pharmacological activation of the LXR pathway (Figure 7H). The region containing peak 3 was also cloned but did not respond to IL-4 in transfection studies. In order to know whether the inhibitory action on IRF4 could help explain the effects of LXR agonists on *Ccl17* expression, we assessed the consequences of IRF4 overexpression in transfected cells. Interestingly, the overexpression of IRF4 up-regulated the activity of *Ccl17* enhancer 2 in the absence of IL-4 and counteracted the inhibitory action of LXR agonists (Figure 7H), thus

supporting the crosstalk between LXRs and IRF4 as a mechanism mediating the control of *Ccl17* expression.

Provided the inhibitory effects of LXR agonists on *Ccl17* expression in TAMs (Figure 4A-C), we further explored whether LXR activation resulted in decreased IRF4 expression in these cells. Interestingly, a decline was observed in the levels of *Irf4* in MHCII^{high} TAMs from T1317-treated tumors (Figure 7I) in WT mice but not in LXR-deficient mice (Figure 7J). In addition, *Irf4* expression was significantly inhibited in MHCII^{high} TAMs and MHCII^{low} TAMs treated *ex vivo* with T1317 (Figure 7K). Of note, as is the case for *Ccl17*, the levels of *Irf4* expression dropped down drastically when MHCII^{high} TAMs were cultured *in vitro*. Taken together, these results suggest that the inhibitory action of the LXR agonist on IRF4 expression may contribute to reduce the levels of CCL17 in the tumor microenvironment. Importantly, pharmacological activation of the LXR pathway also inhibited the induction of *Ccl17*, *Ccl22* and *Irf4* by IL-4 in human macrophages (Figure 7L), suggesting that this crosstalk is evolutionary conserved and may also be relevant in humans.

To determine whether functional IRF4 expression is important for the anti-tumoral actions of the LXR agonist *in vivo*, tumor progression studies were carried out in WT and IRF4$^{-/-}$ mice treated with either DMSO or T1317. Tumors acquired larger volumes in IRF4$^{-/-}$ mice as compared to WT mice (Figure 7M). Notably, there was lower infiltration of lymphocytes in general (not only Tregs) in the tumors in IRF4$^{-/-}$ mice (Figure 7N), which may explain the increased tumor growth in these mice. Nevertheless, the tumors in the IRF4$^{-/-}$ background were not as responsive to T1317 as the tumors grown in WT mice, which supports the importance of IRF4 as a mediator of the anti-tumoral actions of pharmacological LXR activation.

Discussion

In this study we have identified novel roles of activated LXRs in the control of tumor growth. Despite the fact that the synthetic LXR agonist T1317 is able to directly inhibit cancer cell proliferation *in vitro*, its anti-tumoral potential is compromised in LXR-deficient mice carrying WT tumors, thus highlighting the importance of LXR functional activity in the tumor microenvironment over direct anti-proliferative effects in a cancer cell-autonomous manner. Indeed, most studies, including ours, have only demonstrated significant effects of LXR agonists at directly inhibiting the proliferation of transformed cells when used at relatively high doses (5-10 μM) (47–49), in contrast to lower doses required for the activation of metabolic pathways or for the repression of inflammatory gene expression in primary cells.

Previous work by Tavazoie et al. also placed the focus on the role of LXRs in the tumor microenvironment by showing the down-regulation of the frequency of MDSCs and an increased CTL activity within tumors in response to high doses of LXR agonists (11). Mechanistic studies using melanoma B16F10 cells indicated that LXR activation, in an *ApoE*-dependent manner, resulted in increased apoptosis of MDSCs. In the work presented here, the characterization of infiltrated myeloid cells from lung carcinoma tumors indicated that LXR agonism slightly reduced the relative frequency of $MHCII^{high}$ TAMs without affecting other, more abundant populations in the tumor, including those populations theoretically enriched for MDSCs. It is possible that differences in the type of tumor, in the type of agonist, or in the stage of tumor progression at the time of agonist administration help explain why MDSC frequencies were not decreased in our model. In addition, the dose of agonist used during development of LLC tumors in our

study was considerably lower (15 mg/kg/day) than the doses at which LXR agonists inhibited intratumoral MDSC frequencies (80-100 mg/kg/day) in the work mentioned above. In this sense, *ApoE* mRNA levels were not up-regulated in whole tumors from mice treated with the dose of T1317 used in our study nor in TAMs exposed to the agonist *in vitro*, in contrast to the increase in other well established LXR targets genes.

TAMs may locally expand in response to M-CSF (50). Although it is not clear which signals specifically modulate the proliferation or survival of MHCII^{high} TAMs, we have previously shown that LXR agonists inhibit macrophage proliferation induced by several growth factors, including M-CSF and GM-CSF (37). For these reasons, we cannot discard some contribution of the LXR pathway to the control of local TAM proliferation. However, the decreased proportion of MHCII^{high} TAMs was not consistently accompanied by reduced absolute numbers of these cells within the tumor, which suggests that the changes in their frequency are mostly influenced by the relative distribution of other intratumoral cells.

The results from this work strongly suggest that combined actions that result from the modulation of TAM responses contribute to the anti-tumoral effects of pharmacological LXR activation. The LXR agonist is able to repress several genes that play key roles in the pro-tumoral program of TAMs. In fact, the capability of TAMs to suppress T cell proliferation *in vitro* was reduced by the LXR agonist. Notably, different subsets of genes were repressed by T1317 in MHCII^{high} TAMs and MHCII^{low} TAMs. For example, *Nos2* expression was selectively repressed in MHCII^{high} TAMs, whereas *Trem1* expression was inhibited in MHCII^{low} TAMs. We do not have a clear explanation for these differences, but we cannot discard that hypoxic conditions may result in intracellular changes increasing the resistance of some genes to LXR-mediated

repression. In addition, previous work has reported differences in the mechanisms used by these two subpopulations to suppress T cell activation, with MHCII^{high} TAMs being more dependent on NOS2 activity (21). Therefore, further understanding of the relative contribution of some of these genes in the suppressive activity of TAM subpopulations is still warranted.

In addition to direct suppressive mechanisms, MHCII^{high} TAMs are major contributors to CCL17 and CCL22 production (21), which are important signals for Treg recruitment to the tumor. The analysis of the actions of the LXR agonist on TAM subpopulations *in vivo* showed the significant repression of *Ccl17* in MHCII^{high} TAMs and a tendency for such repression in MHCII^{low} TAMs. The effects of the LXR agonist on the latter population were more evident when the cells were exposed to the agonist *ex vivo*, suggesting that the availability of the LXR ligand might be lower in hypoxic areas of the tumor. Treatment with the LXR agonist did not impact the frequency of Tregs in the spleen or their capacity to proliferate *in vitro*, which supports the notion that the repression of CCL17 production in TAMs has an important role in the reduction of the abundance of intratumoral Tregs upon LXR activation. Despite the fact that Tregs exist in low numbers in LLC tumors, depletion of these cells *in vivo* diminished tumor progression in mice. Importantly, the pharmacological activation of LXRs did not efficiently reduce tumor growth under these conditions, suggesting that the inhibitory effects on Treg abundance are an important mechanism mediating the anti-tumoral actions of the LXR agonist. Since LXR activation did not inhibit functional aspects on isolated Tregs, such as the expression of anti-inflammatory cytokines or their capacity to suppress T cell proliferation *ex vivo*, we conclude that the importance of this mechanism lies in the ability of the LXR agonist to downregulate the abundance of

Tregs within the tumor, in correlation with reduced chemokine expression by TAMs, rather than in compromising the immunosuppressive potential of the Treg itself.

Our *in vitro* studies indicate that, in the absence of a synthetic LXR agonist, saturating doses of recombinant IL-4 or GM-CSF are able to induce higher production of CCL17/22 in LXR-deficient macrophages than in the WT counterparts. However, within a more complex entity, the tumor microenvironment, WT and LXR-deficient MHCII^{high} TAMs express similar levels of these chemokines in the absence of pharmacological LXR activation, in line with the fact that tumors grown in LXR-deficient mice do not display a drastic increase in Treg abundance. Therefore, whether or not LXR-deficient cells produce higher levels of the chemokine might depend on additional signals that are present in each setting. Similar observations in other cellular/physiological scenarios (5,11,51,52) support the notions that LXR biology is complex and that genetic ablation and pharmacological activation of these nuclear receptors do not necessarily result in opposite biological effects.

At the molecular level, the results from this work propose IRF4 targeting as a relevant mechanism that links pharmacological LXR activation with the downregulation of *Ccl17*. On one hand, the induction of this chemokine by IL-4 or GM-CSF is fully dependent on IRF4 functionality, and LXR activity is able to downregulate IRF4 expression in both settings. On the other hand, IRF4 overexpression blocked the capability of LXR agonists to negatively modulate the transcriptional enhancing activity of a region containing IRF4 binding sites upstream of the *Ccl17* promoter (and downstream of *Ccl22*). It is plausible that the down-regulation of IRF4 expression may also contribute to the repressive actions of LXR agonists on other genes induced by GM-CSF.

Within tumors, in correlation with the inhibitory effects on *Ccl17* expression, the levels of *Irf4* were down-regulated in MHCII^{high} TAMs in response to the administration of the LXR agonist *in vivo*. However, interpretation of the data from the systemic deficiency in IRF4 should be done with caution. IRF4 is involved in the development and function of different subsets of $CD4^+$ T cells, not only Tregs, and in the generation of Th1 responses (reviewed in (53). The reduced infiltration of $CD8^+$ and $CD4^+$ lymphocytes in LLC tumors most probably compromises the development of anti-tumoral immune responses, which would explain the increased tumor growth in the IRF4-deficient model despite Treg numbers being downregulated. In line with this notion, systemic IRF4 deficiency promoted an immunosuppressed tumor microenvironment in other models of cancer (54). Importantly, these mice did not respond to pharmacological LXR activation as efficiently as WT mice, which suggests that IRF4 plays a relevant role in the anti-tumoral actions of the LXR agonist. However, we are aware that a deficiency of IRF4 specifically in macrophages would help to better answer this question. Future studies will be addressed in this direction.

In this work we have validated that pharmacological activation of LXRs also exerts inhibitory effects on the induction of the *Irf4*/*Ccl17* axis in human macrophages. However, whether or not the expression levels of *Irf4* specifically in TAMs have prognostic value in human tumors remains elusive. Importantly, the accumulation of CCL17-expressing macrophages has been described in lung adenocarcinoma, favoring the recruitment of effector Tregs (55). In addition, high expression levels of intratumoral CCL17 have been associated with poorer overall survival rates in hepatocellular carcinoma (56). Moreover, Kaplan-Meier analysis using the R2: Genomics Analysis and Visualization Platform (http://r2.amc.nl) to assess the probability of overall survival in patient cohorts of kidney renal clear cell carcinoma

from The Cancer Genome Atlas project, as well as in non-small cell lung cancer (57), indicates that high expression of CCL17 also associates with poorer overall survival probability in these types of cancer (Supplemental Figure S8). On the other side, in a mouse model of subcutaneous tumor development, the downregulation of CCL17 upon transduction of short hairpin RNA in CT26 cancer cells resulted in decreased Treg infiltration within tumors and suppressed tumor growth (58), suggesting that targeting the intratumoral levels of CCL17 may represent a promising strategy against cancer.

Taken together, this work reveals unappreciated roles for pharmacological LXR activation in the control of several macrophage-mediated mechanisms contributing to the maintenance of an immunosuppressive microenvironment, thus providing novel insights about the mechanisms of action of LXR agonists as therapeutic drugs against cancer.

Acknowledgments

We thank D. Mangelsdorf for the LXR-deficient mice, A. Celada for anti-phospho STAT6 antibodies, D. Baltimore for making the plasmid pMIG-IRF4 available, and M. García, C. Izquierdo and E. Glaría for technical assistance. This work was supported by the following grants: Spanish Ministry of Economy and Competitivity (MINECO) grants SAF2017-89510-R and SAF2014-57856-P to A.F.V. and C.C., SAF2014-56819-R to A.C., SAF2017-90604-REDT and SAF2015-71878-REDT to the NuRCaMeIn network (A.F.V., C.C. and A.C.); Spanish Ministry of Science and Innovation (MICINN) grants SAF2011-23402 and SAF2010-14989 to A.F.V.; Fundació La Marató de TV3 grant 080930 to A.F.V.; grants DFG HU 1824/5-1, 1824/7-1 and 1824/9-1 to

MH; the European Cooperation in Science and Technology (COST) Action BM1404 Mye-EUNITER (http://www.mye-eunit er.eu) (A.F.V., J.v.G.); and Instituto de Salud Carlos III and FEDER “Una manera de hacer Europa” grant FIS 16/00139 to J.C.E-G. CIBERDEM is an Instituto de Salud Carlos III project. J.M.C. received a fellowship from the University of Barcelona (APIF) and J.F.D. received a fellowship from the Spanish Ministry of Science, Innovation and Universities (FPI, PRE2018-085579).

Author Contributions

Conception and design: JMC, TEL, JFD, JAVG, AFV; Development of methodology: JMC, TEL, JFD, FRP, DS, MH, LiCe, JCEG, TS, JAVG, AFV; Acquisition of data: JMC, TEL, JFD, FRP, DS, LiCe, AFV; Analysis and interpretation of data: JMC, TEL, JFD, JVD, AC, FRP, DS, MH, LiCe, JCEG, CC, AFV; Writing-original draft: JMC, TEL, JFD, AFV; Writing-review and editing: JMC, TL, JFD, CC, JAVG, AVF; Material support: AC, LuCa, MH, LB, TS, EFW; Study supervision: CC, AFV.

References

1. Schulman IG. Liver X receptors link lipid metabolism and inflammation. FEBS Lett. 2017. page 2978–91.
2. A-Gonzalez N, Bensinger SJ, Hong C, Beceiro S, Bradley MN, Zelcer N, et al. Apoptotic cells promote their own clearance and immune tolerance through activation of the nuclear receptor LXR. Immunity. 2009;31:245–58.
3. Feig JE, Pineda-Torra I, Sanson M, Bradley MN, Vengrenyuk Y, Bogunovic D, et al. LXR promotes the maximal egress of monocyte-derived cells from mouse aortic plaques during atherosclerosis regression. J Clin Invest. 2010;120:4415–24.
4. Joseph SB, Bradley MN, Castrillo A, Bruhn KW, Mak PA, Pei L, et al. LXR-dependent gene expression is important for macrophage survival and the innate immune response. Cell. 2004;119:299–309.
5. Matalonga J, Glaria E, Bresque M, Escande C, Carbó JM, Kiefer K, et al. The Nuclear Receptor LXR Limits Bacterial Infection of Host Macrophages through a Mechanism that Impacts Cellular NAD Metabolism. Cell Rep. 2017;18:1241–55.
6. Valledor AF, Hsu LC, Ogawa S, Sawka-Verhelle D, Karin M, Glass CK. Activation of liver X receptors and retinoid X receptors prevents bacterial-induced macrophage apoptosis. Proc Natl Acad Sci U S A. 2004;101:17813–8.
7. Steffensen KR, Jakobsson T, Gustafsson J-Å. Targeting liver X receptors in inflammation. Expert Opin Ther Targets. Taylor & Francis; 2013;17:977–90.
8. Lin C-Y, Gustafsson J-Å. Targeting liver X receptors in cancer therapeutics. Nat Rev Cancer. 2015;15:216–24.
9. Pencheva N, Buss CG, Posada J, Merghoub T, Tavazoie SF. Broad-Spectrum Therapeutic Suppression of Metastatic Melanoma through Nuclear Hormone Receptor Activation. Cell. 2014;156:986–1001.
10. Nelson ER, Wardell SE, Jasper JS, Park S, Suchindran S, Howe MK, et al. 27-Hydroxycholesterol Links Hypercholesterolemia and Breast Cancer Pathophysiology. Science (80-). 2013;342.
11. Tavazoie MF, Pollack I, Tanqueco R, Ostendorf BN, Reis BS, Gonsalves FC, et al. LXR/ApoE Activation Restricts Innate Immune Suppression in Cancer. Cell. 2018;172:825-840.e18.
12. Villablanca EJ, Raccosta L, Zhou D, Fontana R, Maggioni D, Negro A, et al. Tumor - mediated liver X receptor - α activation inhibits CC chemokine receptor - 7 expression on dendritic cells and dampens antitumor responses. Nat Med. Nature Publishing Group; 2009;16:98–105.
13. Zhang C, Lei G-S, Shao S, Jung H-W, Durant PJ, Lee C-H. Accumulation of myeloid-derived suppressor cells in the lungs during Pneumocystis pneumonia. Infect Immun. American Society for Microbiology (ASM); 2012;80:3634–41.
14. Campbell MJ, Tonlaar NY, Garwood ER, Huo D, Moore DH, Khramtsov AI, et al. Proliferating macrophages associated with high grade, hormone receptor negative breast cancer and poor clinical outcome. Breast Cancer Res Treat. 2011;128:703–11.

15. Mantovani A, Sica A. Macrophages, innate immunity and cancer: balance, tolerance, and diversity. Curr Opin Immunol. 2010;22:231–7.

16. Noy R, Pollard JW. Tumor-associated macrophages: from mechanisms to therapy. Immunity. 2014;41:49–61.

17. Su S, Liu Q, Chen J, Chen J, Chen F, He C, et al. A positive feedback loop between mesenchymal-like cancer cells and macrophages is essential to breast cancer metastasis. Cancer Cell. 2014;25:605–20.

18. Van Overmeire E, Stijlemans B, Heymann F, Keirsse J, Morias Y, Elkrim Y, et al. M-CSF and GM-CSF Receptor Signaling Differentially Regulate Monocyte Maturation and Macrophage Polarization in the Tumor Microenvironment. Cancer Res. 2016;76:35–42.

19. Curiel TJ, Coukos G, Zou L, Alvarez X, Cheng P, Mottram P, et al. Specific recruitment of regulatory T cells in ovarian carcinoma fosters immune privilege and predicts reduced survival. Nat Med. Nature Publishing Group; 2004;10:942–9.

20. Ishida T, Ueda R. CCR4 as a novel molecular target for immunotherapy of cancer. Cancer Sci. 2006;97:1139–46.

21. Movahedi K, Laoui D, Gysemans C, Baeten M, Stange G, Van den Bossche J, et al. Different Tumor Microenvironments Contain Functionally Distinct Subsets of Macrophages Derived from Ly6C(high) Monocytes. Cancer Res. 2010;70:5728–39.

22. Laoui D, Van Overmeire E, Di Conza G, Aldeni C, Keirsse J, Morias Y, et al. Tumor Hypoxia Does Not Drive Differentiation of Tumor-Associated Macrophages but Rather Fine-Tunes the M2-like Macrophage Population. Cancer Res. 2014;74:24–30.

23. Presa M, Ortiz AZ, Garabatos N, Izquierdo C, Rivas EI, Teyton L, et al. Cholera toxin subunit B peptide fusion proteins reveal impaired oral tolerance induction in diabetes-prone but not in diabetes-resistant mice. Eur J Immunol. NIH Public Access; 2013;43:2969–79.

24. Guy CT, Cardiff RD, Muller WJ. Induction of mammary tumors by expression of polyomavirus middle T oncogene: a transgenic mouse model for metastatic disease. Mol Cell Biol. 1992;12:954–61.

25. Thomsen MK, Bakiri L, Hasenfuss SC, Hamacher R, Martinez L, Wagner EF. JUNB/AP-1 controls IFN-γ during inflammatory liver disease. J Clin Invest. 2013;123:5258–68.

26. Thépot D, Weitzman JB, Barra J, Segretain D, Stinnakre MG, Babinet C, et al. Targeted disruption of the murine junD gene results in multiple defects in male reproductive function. Development. 2000;127:143–53.

27. Valledor AF, Comalada M, Xaus J, Celada A. The differential time-course of extracellular-regulated kinase activity correlates with the macrophage response toward proliferation or activation. J Biol Chem. 2000;275:7403–9.

28. Remels LM, De Baetselier PC. Characterization of 3LL-tumor variants generated by in vitro macrophage-mediated selection. Int J cancer. 1987;39:343–52.

29. Casazza A, Laoui D, Wenes M, Rizzolio S, Bassani N, Mambretti M, et al. Impeding Macrophage Entry into Hypoxic Tumor Areas by Sema3A/Nrp1

Signaling Blockade Inhibits Angiogenesis and Restores Antitumor Immunity. Cancer Cell. 2013;24:695–709.

30. Cedó L, García-León A, Baila-Rueda L, Santos D, Grijalva V, Martínez-Cignoni MR, et al. ApoA-I mimetic administration, but not increased apoA-I-containing HDL, inhibits tumour growth in a mouse model of inherited breast cancer. Sci Rep. 2016;6.

31. Izquierdo C, Ortiz AZ, Presa M, Malo S, Montoya A, Garabatos N, et al. Treatment of T1D via optimized expansion of antigen-specific Tregs induced by IL-2/anti-IL-2 monoclonal antibody complexes and peptide/MHC tetramers. Sci Rep. Nature Publishing Group; 2018;8:1–14.

32. Mi H, Huang X, Muruganujan A, Tang H, Mills C, Kang D, et al. PANTHER version 11: expanded annotation data from Gene Ontology and Reactome pathways, and data analysis tool enhancements. Nucleic Acids Res. Oxford University Press; 2017;45:D183–9.

33. Ciofani M, Madar A, Galan C, Sellars M, Mace K, Pauli F, et al. A Validated Regulatory Network for Th17 Cell Specification. Cell. 2012;151:289–303.

34. Yang J, Chen X, McDermaid A, Ma Q. DMINDA 2.0: integrated and systematic views of regulatory DNA motif identification and analyses. Hancock J, editor. Bioinformatics. 2017;33:2586–8.

35. So AYL, Sookram R, Chaudhuri AA, Minisandram A, Cheng D, Xie C, et al. Dual mechanisms by which miR-125b represses IRF4 to induce myeloid and B-cell leukemias. Blood. American Society of Hematology; 2014;124:1502–12.

36. Bensinger SJ, Bradley MN, Joseph SB, Zelcer N, Janssen EM, Hausner MA, et al. LXR signaling couples sterol metabolism to proliferation in the acquired immune response. Cell. 2008;134:97–111.

37. Pascual-García M, Carbó JM, León T, Matalonga J, Out R, Berkel TV, et al. Liver X receptors inhibit macrophage proliferation through downregulation of cyclins D1 and B1 and cyclin-dependent kinases 2 and 4. J Immunol. 2011;186.

38. Tanaka A, Sakaguchi S. Regulatory T cells in cancer immunotherapy. Cell Res. 2017;27:109–18.

39. Mizukami Y, Kono K, Kawaguchi Y, Akaike H, Kamimura K, Sugai H, et al. CCL17 and CCL22 chemokines within tumor microenvironment are related to accumulation of Foxp3+ regulatory T cells in gastric cancer. Int J cancer. 2008;122:2286–93.

40. Andrew DP, Chang MS, McNinch J, Wathen ST, Rihanek M, Tseng J, et al. STCP-1 (MDC) CC chemokine acts specifically on chronically activated Th2 lymphocytes and is produced by monocytes on stimulation with Th2 cytokines IL-4 and IL-13. J Immunol. 1998;161:5027–38.

41. Lacey DC, Achuthan A, Fleetwood AJ, Dinh H, Roiniotis J, Scholz GM, et al. Defining GM-CSF- and Macrophage-CSF-Dependent Macrophage Responses by In Vitro Models. J Immunol. 2012;188:5752–65.

42. Pechkovsky D V., Prasse A, Kollert F, Engel KMY, Dentler J, Luttmann W, et al. Alternatively activated alveolar macrophages in pulmonary fibrosis—mediator production and intracellular signal transduction. Clin Immunol. Academic Press; 2010;137:89–101.

43. El Chartouni C, Schwarzfischer L, Rehli M. Interleukin-4 induced interferon regulatory factor (Irf) 4 participates in the regulation of alternative macrophage priming. Immunobiology. 2010;215:821–5.

44. Li P, Spolski R, Liao W, Wang L, Murphy TL, Murphy KM, et al. BATF–JUN is critical for IRF4-mediated transcription in T cells. Nature. 2012;490:543–6.

45. Achuthan A, Cook AD, Lee MC, Saleh R, Khiew HW, Chang MWN, et al. Granulocyte macrophage colony-stimulating factor induces CCL17 production via IRF4 to mediate inflammation. J Clin Invest. 2016;126:3453–66.

46. Hsu AT, Lupancu TJ, Lee M-C, Fleetwood AJ, Cook AD, Hamilton JA, et al. Epigenetic and transcriptional regulation of IL4-induced CCL17 production in human monocytes and murine macrophages. J Biol Chem. 2018;293:11415–23.

47. Fukuchi J, Hiipakka RA, Kokontis JM, Hsu S, Ko AL, Fitzgerald ML, et al. Androgenic suppression of ATP-binding cassette transporter A1 expression in LNCaP human prostate cancer cells. Cancer Res. 2004;64:7682–5.

48. Rough JJ, Monroy MA, Yerrum S, Daly JM. Anti-proliferative effect of LXR agonist T0901317 in ovarian carcinoma cells. J Ovarian Res. 2010;3:13.

49. Vedin L-L, Lewandowski SA, Parini P, Gustafsson J-A, Steffensen KR. The oxysterol receptor LXR inhibits proliferation of human breast cancer cells. Carcinogenesis. 2009;30:575–9.

50. Tymoszuk P, Evens H, Marzola V, Wachowicz K, Wasmer M-H, Datta S, et al. In situ proliferation contributes to accumulation of tumor-associated macrophages in spontaneous mammary tumors. Eur J Immunol. 2014;44:2247–62.

51. Saini SPS, Zhang B, Niu Y, Jiang M, Gao J, Zhai Y, et al. Activation of liver X receptor increases acetaminophen clearance and prevents its toxicity in mice. Hepatology. John Wiley & Sons, Ltd; 2011;54:2208–17.

52. Pourcet B, Gage MC, Leon TE, Waddington KE, Pello OM, Steffensen KR, et al. The nuclear receptor LXR modulates interleukin-18 levels in macrophages through multiple mechanisms. Sci Rep. 2016;6:25481.

53. Crepeau RL, Ford ML. Programmed T cell differentiation: Implications for transplantation. Cell. Immunol. Academic Press Inc.; 2020. page 104099.

54. Metzger P, Kirchleitner S V., Boehmer DFR, Hörth C, Eisele A, Ormanns S, et al. Systemic but not MDSC-specific IRF4 deficiency promotes an immunosuppressed tumor microenvironment in a murine pancreatic cancer model. Cancer Immunol Immunother. Springer Science and Business Media Deutschland GmbH; 2020;69:2101–12.

55. Kinoshita T, Kudo-Saito C, Muramatsu R, Fujita T, Saito M, Nagumo H, et al. Determination of poor prognostic immune features of tumour microenvironment in non-smoking patients with lung adenocarcinoma. Eur J Cancer. 2017;86:15–27.

56. Zhu F, Li X, Chen S, Zeng Q, Zhao Y, Luo F. Tumor-associated macrophage or chemokine ligand CCL17 positively regulates the tumorigenesis of hepatocellular carcinoma. Med Oncol. 2016;33:17.

57. Bild AH, Yao G, Chang JT, Wang Q, Potti A, Chasse D, et al. Oncogenic pathway signatures in human cancers as a guide to targeted therapies. Nature.

Nature Publishing Group; 2006;439:353–7.

58. Hirata A, Hashimoto H, Shibasaki C, Narumi K, Aoki K. Intratumoral IFN-α gene delivery reduces tumor-infiltrating regulatory T cells through the downregulation of tumor CCL17 expression. Cancer Gene Ther. Nature Publishing Group; 2019;26:334–43.

Figure legends

Figure 1. Functional LXR expression in host cells is essential for the anti-tumoral actions of the LXR agonist T1317. A) 3LL-R cells express LXRα and β, as measured by qPCR. Expression values normalized to the expression levels of L14. Data represent mean ± SEM; n = 4 independent experiments. **B)** LXR agonists inhibit 3LL-R cell proliferation *in vitro*. 3LL-R cells were starved for 24 h in RPMI without FCS in the presence of either vehicle (DMSO) or the indicated concentrations of LXR agonists, T1317 or GW3965. Cell proliferation was induced during 24 h in the presence of 10 % FCS and 0.3g/L L-Gln, whereas control cells were kept in RPMI alone. In all samples, ^{3}H-thymidine was added for 6 h. After cell lysis, ^{3}H-thymidine incorporation was measured as an indication of DNA synthesis. Data represent mean ± SD from a representative experiment performed in triplicates. ANOVA-Bonferroni. *, $p < 0.05$; ***, $p < 0.001$. Similar results were obtained in n = 3 independent experiments. **C-D)** WT (**C)** or LXRα/β$^{-/-}$ (**D**) male mice were subjected to the subcutaneous injection of $3x10^{6}$ 3LL-R cells. From day 7 after tumor cell injection, the mice were treated daily (intraperitoneal injection) with either vehicle (DMSO) or the LXR agonist T1317 (15 mg/kg). Tumor volume was measured daily up to day 15. Mean ± SEM; n = 14 (**C**), n = 9 (**D**). Two-way ANOVA with repeated measures. In **E-G**, PyMT female mice were administered a chow diet with or without supplementation with T1317 (50 mg/kg) right after weaning. Tumor latency was evaluated daily; Log-Rank-Wilcoxon test (**E**). At 22 weeks of age the mice were sacrificed and the weight was measured for each mammary gland (**F**). Total mammary gland weight is represented in **G**. Mean ± SEM; n = 8 (Control), n = 10 (T1317). Mann–Whitney U test. *, $p < 0.05$; **, $p < 0.01$; ***, $p < 0.001$.

Figure 2. Pharmacological stimulation of the LXR pathway reduces the abundance of Tregs in the tumor. WT C57BL/6 mice (**A**, **B**, **D**, **F, G**), Foxp3EGFP transgenic mice (**C**) or LXR-deficient mice (**F**) were subjected to subcutaneous injection of 3LL-R cells. The mice were treated daily with DMSO or T1317 (15 mg/kg) from day 7 (**A**, **B**, **D**, **F, G**) or day 5 (**C**) of tumor establishment. The tumors were collected at day 15 (**A**, **B**, **D**, **F**) or day 10 (**C**) after tumor inoculation. The spleens were collected at day 15 (**G**). The abundance of different immune cell populations was measured by flow cytometry. In **A**-**C** and **G**, the graphics represent the frequencies of immune cell populations (percentage of gated live singlets) in the tumors (**A**-**C**) or spleens (**G**). Horizontal bars indicate mean values from each experimental group. Pooled data from two (**B**, **G**) or three (**A**, **C**) independent experiments; n = 18-19 (**A**), n = 11-12 (**B, C**), n = 10-11 (**G**) mice/group. Mann-Whitney test. In **D**, the absolute amount of Tregs was determined in each tumor and normalized to the tumor volume. Pooled data from two independent experiments; n = 10-11 mice/group. T-test. In **E**, PyMT female mice were administered a chow diet with or without supplementation with T1317 (50 mg/kg). Relative expression levels of *Foxp3* mRNA (normalized to L14) in mammary glands at 22 weeks of age. qPCR. n = 8-10 mice/group. T-test. In **F**, the absolute numbers of intratumoral immune cells normalized to the tumor weight was determined in WT and LXR-deficient mice. n = 5 mice/group. One-way ANOVA test followed by Newman-Keuls post hoc. *, $p < 0.05$; ***, $p < 0.001$

Figure 3. The anti-tumoral action of T1317 is not effective in mice undergoing Treg depletion. A) T1317 does not impair the capability of Tregs to suppress T cell proliferation. Tregs were isolated from the spleens (left panel) or tumors (right panel) of

Foxp3EGFP mice. Total splenocytes were isolated from the spleens of WT mice, stained with CFSE and incubated with Tregs at a 1:1 (Treg:splenocyte) ratio. Control cells were grown in the absence of Tregs. T cell proliferation was induced *in vitro* for 48 h using antibodies against CD3ε and CD28 and analyzed by flow cytometry. The graphics represent the percentage of cells with CFSE dispersion compared to non-activated splenocytes. Mean ± SD. Left panel, n = 3 biological replicates. Right panel, n = 5 biological replicates (pooled data from two independent experiments). T-test. *, $p < 0.05$; **, $p < 0.01$. **B-C**) Tregs were isolated from the spleen of Foxp3EGFP. In **B**, purified Tregs were incubated with DMSO or T1317 *in vitro* and the expression of *Il10* and *Tgfb* was analyzed by qPCR; Mean ± SD, n = 3. In **C**, Tregs were stained with CFSE, incubated with DMSO or T1317 and induced to proliferate in the presence of a combination of anti-CD3/CD28 antibodies and murine recombinant IL-2 (100 U/ml). Mean ± SD, n = 3. One-way ANOVA. **D-E**) Male Foxp3EGFP reporter mice were subjected to the subcutaneous injection of $3x10^6$ 3LL-R cells. At days 2, 5 and 8 post-tumor cell injection, the mice were administered either antibodies anti-CD25 or control isotype antibodies (200 μg per animal in PBS by intra-peritoneal injection). At day 5, and until day 9, the mice received a daily dose of T1317 (15 mg/kg) or vehicle (DMSO). n=5-6 animals/group. **D**) At day 10, the mice were euthanized. The frequency of FoxP3-GFP^+ Treg in spleens (upper panel) and tumors (lower panel) was evaluated by flow cytometry. Horizontal bars represent mean values. Kruskal-Wallis test followed by Dunn's multiple comparison test; *, $p < 0.05$; **, $p < 0.01$. Selected experimental conditions were also compared using a Mann-Whitney test; #, $p < 0.05$; ##, $p < 0.01$. **E**) Tumor volumes were measured from day 5 to day 10 and represented as fold change. Two-way ANOVA with repeated measures. *, $p < 0.05$; **, $p < 0.01$; ***, $p < 0.001$.

Figure 4. Pharmacological LXR activation downregulates the expression of genes that are part of the pro-tumoral program of TAMs. A-B) WT (**A**) or LXR-deficient (**B**) male mice were treated daily with DMSO or T1317 (15 mg/kg) from day 7 of tumor establishment. MHCII^{high} and MHCII^{low} TAMs were isolated at day 15 after tumor cell inoculation. **C-G**) MHCII^{high} and MHCII^{low} TAMs were isolated from 15-day tumors and stimulated *ex vivo* with T1317 (1 μM) or DMSO for 18 h (**D-E**) or 24 h (**C, F-G**). In **A-C**, the expression of *Ccl17* and *Ccl22* was analyzed by qPCR. Mean ± SEM. In **A**, n = 5 mice/group. In **B**, n = 7-8 mice/group; pooled data from two independent experiments. In **C**, n = 3-5 experiments (each using 4-5 pooled male mice). In **A-C**, T-test. *, $p < 0.05$; **, $p < 0.01$. **D**) LXR activation inhibits the capability of TAMs to suppress T cell proliferation. Freshly isolated splenocytes were stained with CFSE and incubated with TAMs at a 1:1 (TAM:splenocyte) ratio. Control cells were maintained in the absence of TAMs. T cell proliferation was induced for 48 h using antibodies against CD3ε and CD28 and analyzed by flow cytometry. The graphic represents the percentage of cells with CFSE dispersion using non-activated splenocytes as reference. Mean ± SD; n = 3 biological replicates. One-way ANOVA. *, $p < 0.05$; ***, $p < 0.001$. **E**) TAMs were incubated with 3 μm fluorescent microspheres (20 beads/cell) for 30 min. The phagocytosis of microspheres was analyzed by flow cytometry. Mean ± SD; n = 2 biological replicates. **F**) Changes in gene expression were analyzed by gene profiling. The results from three (MHCII^{high} TAMs) or two (MHCII^{low} TAMs) independent experiments are included. The graphic shows the percentage of repression by T1317 of genes that have been selected because of their reported involvement in immunosuppressive functions in the tumor microenvironment or in macrophage alternative activation. Paired T-test. **G**) The selective repression of several genes in MHCII^{high} TAMs was validated through qPCR. Mean ± SEM, n = 3 independent

experiments. T-test. In **F**-**G**, *, $p < 0.05$; **, $p < 0.01$; ***, $p < 0.001$ (T1317-treated *versus* control cells).

Figure 5. Pharmacological LXR activation inhibits the IL-4-mediated induction of *Ccl17* and *Ccl22.* **A**-**E**) Bone marrow derived macrophages were obtained from WT mice (**A**-**B, E**) or LXRα/β$^{-/-}$ mice (**C**-**E**). The cells were stimulated with either vehicle (DMSO), GW3965 (1μM) (**A**, **C**) or T1317 (1μM) (**B**, **D**) for 6 h and then treated with IL-4 (in **A**, **C**: 10 ng/ml during 12, 24 or 36 h; in **B**, **D**: 20 ng/ml for 12 h). In **A**, **C**, similar results were obtained in experiments using more prolonged pre-incubation times with LXR agonists (up to 18 h) and higher doses of IL-4 (up to 20 ng/ml). In **A**-**D**, mean ± SEM; pooled data from n = 3-6 experiments using 1-3 biological replicates/experiment. ANOVA-Bonferroni. *, $p < 0.05$; **, $p < 0.01$; ***, $p < 0.001$. In **A**, a T-test was also used for selected comparisons (#, $p < 0.05$; ##, $p < 0.01$). **E**) Determination of the secreted levels of CCL17 and CCL22 in the supernatants of WT and LXRα/β$^{-/-}$ macrophages stimulated with IL-4 (10 ng/ml, 24 h) in the presence or absence of T1317 (1 μM, pretreatment 16 h). ELISA. Mean ± SD; n = 3 biological replicates. Two-way ANOVA-Bonferroni. *, $p < 0.05$; ***, $p < 0.001$. **F**) The expression curves of *Ccl17* and *Ccl22* in response to IL-4 was compared between WT and LXRα/β$^{-/-}$ macrophages in the absence of LXR agonists. qPCR. Mean ± SEM; n = 4 independent experiments. Two-way ANOVA-Bonferroni. *, $p < 0.05$; **, $p < 0.01$; ***, $p < 0.001$ *versus* WT; ##, $p < 0.01$; ###, $p < 0.001$ *versus* unstimulated cells from each genotype. **G**) The stimulation of WT macrophages with IL-4 did not affect negatively *Lxra* or *Lxrb* mRNA expression, as determined by qPCR. Mean ± SEM, n = 4 independent experiments using 1-3 biological replicates/experiment. ANOVA-Bonferroni. **H**) The activation of LXRs did not interfere with STAT-6 phosphorylation

in response to IL-4. Macrophages were incubated with GW3965 (1 μM, 18 h) or vehicle and then stimulated with IL-4 (20 ng/ml) for the indicated periods of time. Phosphorylated STAT-6 (P-STAT-6) and total STAT-6 were analyzed in whole cell extracts (50 μg/lane) by western blotting using specific antibodies. The same blot was stripped and probed repeatedly.

Figure 6. LXR agonists inhibit the induction of Ccl17 and Ccl22 in response to GM-CSF. Bone marrow-derived macrophages from WT (**A**-**B**, **D**) or LXRα/β$^{-/-}$ (**C**-**D**) mice were treated with vehicle, T1317 or GW3965 (1 μM) for 16 h and then stimulated with GM-CSF (5 ng/ml) for 24 h. In **B**, WT macrophages were treated with GM-CSF for the indicated periods of time. In **A**-**C**, gene expression levels were determined by qPCR. Mean ± SEM. n = 3-8 (**A**), n = 3-4 (**B**), n = 4 (**C**) independent experiments using 1-2 biological replicates/experiment. ANOVA-Bonferroni. In **D**, determination of the secreted levels of CCL17 and CCL22 by ELISA. Mean ± SD; n = 3 biological replicates. Two-way ANOVA-Bonferroni. In **A**-**D**, **, $p < 0.01$; ***, $p < 0.001$. Selected experimental conditions were also compared using a T-test, #, $p < 0.05$; ##, $p < 0.01$.

Figure 7. Pharmacological LXR activation inhibits the induction of *Irf4* by IL-4 or GM-CSF. A-**B**) IRF4 is required for specific gene subsets during the macrophage response to IL-4 or GM-CSF. WT and IRF4-deficient (IRF4$^{-/-}$) macrophages were stimulated with IL-4 (10 ng/ml, 24 h) (**A**) or GM-CSF (5 ng/ml, 24 h) (**B**). Gene expression was analyzed by qPCR. Mean ± SEM, n = 4 independent experiments. Two-way ANOVA-Bonferroni. *, $p < 0.05$; **, $p < 0.01$; ***, $p < 0.001$. In datasets without

factor interaction, selected conditions were compared by T-test, #, $p < 0.05$; ##, $p < 0.01$; ###, $p < 0.001$. **C-G**) LXR inhibits *Irf4* expression. WT (**C-G**) or LXRα/β$^{-/-}$ (**D-E**) macrophages were preincubated with T1317 (**C-G**) or GW3965 (**D-G**) (each at 1 μM, 18 h) and stimulated with IL-4 (10 ng/ml; indicated periods of time in **C** and **F**; 4 h in **D**) or GM-CSF (5 ng/ml; 24 h in **E**; indicated times in **G**). In **C-E**, *Irf4* expression levels were analyzed by qPCR. Mean ± SEM; n = 3 (**C**), n = 6 (**D-E**). ANOVA-Bonferroni (**C, E**), Kruskal-Wallis (**D**). *, $p < 0.05$; **, $p < 0.01$; ***, $p < 0.001$. In **D**, a Mann-Whitney test was also used for selected comparisons (##, $p < 0.01$). In **F-G**, IRF4 expression was analyzed by western blotting (7 μg whole cell extract/lane). In **F-G**, representative experiment. In **F**, two blots were generated in parallel from the same set of samples. In **G**, the same blot was stripped and reprobed. **H**) Raw264.7 macrophages were co-transfected with pGL3-Ccl17 enhancer 2, a plasmid overexpressing LXRα, a plasmid expressing Renilla, and either empty pcDNA3 or a plasmid overexpressing IRF-4. After transfection, the cells were incubated in DMEM-10 % FCS in the presence or absence of LXR agonists T1317 or GW3965 (1 μM, 18 h). Next, the cells were stimulated with IL-4 (10 ng/ml, 24 h). Luciferase activity was measured and normalized to Renilla activity. Mean ± SEM; n = 3 independent experiments. Two-way ANOVA-Bonferroni. **, $p < 0.01$; ***, $p < 0.001$ (*vs* control unstimulated cells); †††, $p < 0.01$ (*vs* the same treatment in the control group). **I-K**) Effects of LXR activation on *Irf4* expression in TAMs. In **I-J**, WT (**I**) or LXRα/β$^{-/-}$ (**J**) male mice were treated daily with DMSO or T1317 (15 mg/kg) from day 7 of tumor establishment. MHCII^{high} and MHCII^{low} TAMs were isolated at day 15 after tumor cell inoculation. In **K**, MHCII^{high} and MHCII^{low} TAMs were isolated from 15-day tumors and stimulated *ex vivo* with T1317 (1 μM) or DMSO for 24 h. In **I-K**, the expression of *Irf4* was analyzed by qPCR. Mean ± SEM, n = 5 mice/group (**I**); n = 6-8 mice/group (pooled data from 2 independent experiments)

(**J**); n = 3 independent experiments (each using 4-5 pooled mice) (**K**). T-test. *, $p < 0.05$. **L**) The treatment of human macrophages with T1317 inhibited the IL-4-induced expression of *Ccl17*, *Ccl22* and *Irf4*. qPCR. n = 3 independent experiments. One-way ANOVA. **M**-**N**) WT or IRF4$^{-/-}$ mice were subjected to subcutaneous injection of 3LL-R cells and treated daily with DMSO or T1317 (15 mg/kg) from day 7 of tumor establishment. In **M**, tumor volume progression curve. In **N**, absolute numbers of intratumoral lymphocytes were measured by flow cytometry and normalized to tumor volume. Mean ± SEM; n = 6-7 mice/group. In **M**, Two-way ANOVA-repeated measures. In **N**, One-way ANOVA – Bonferroni, *, $p < 0.05$; **, $p < 0.01$; ***, $p < 0.001$. Additionally, T-test, #, $p < 0.05$

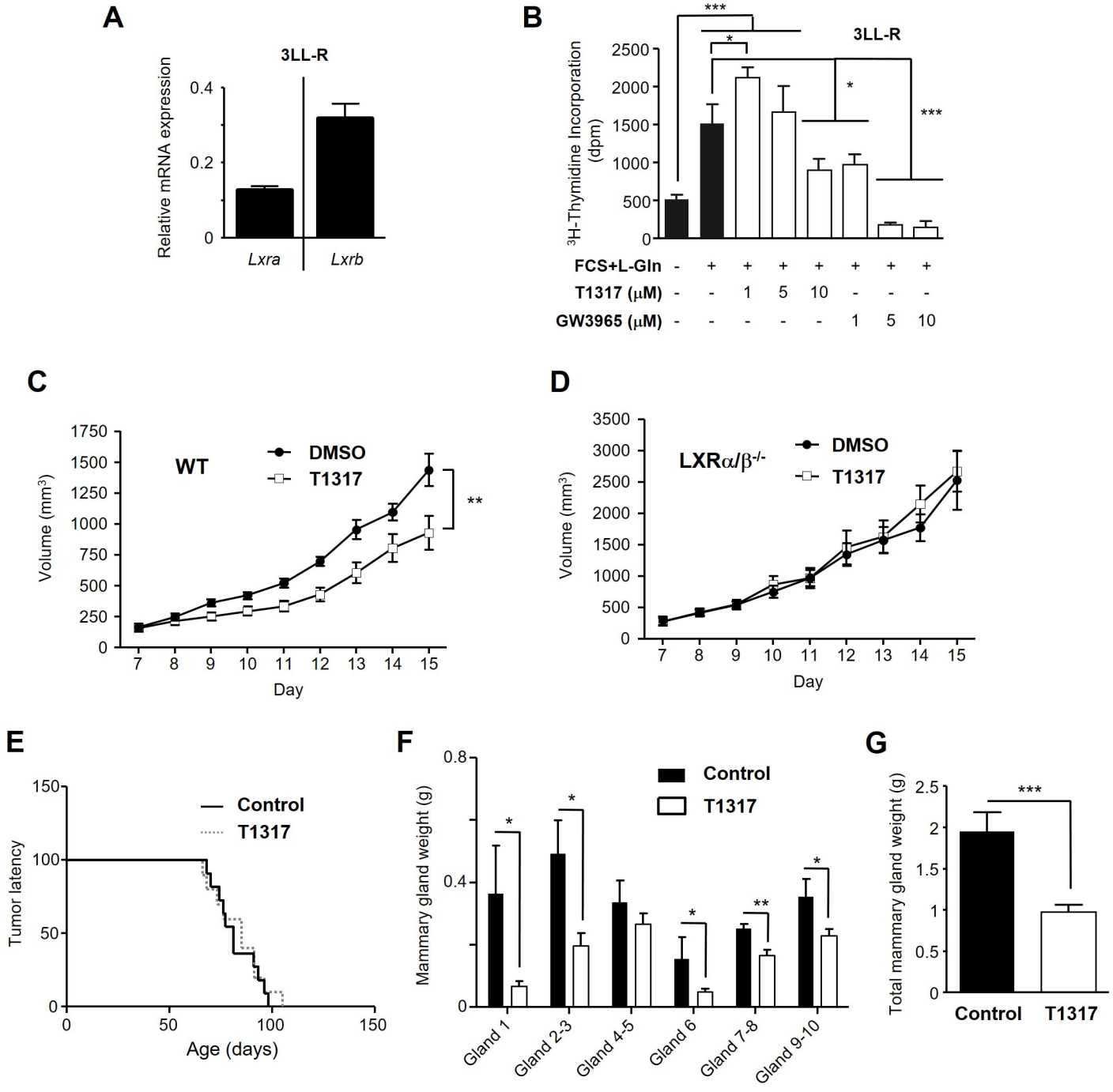
A
3LL-R
Relative mRNA expression
0.4
0.2
0
Lxra
Lxrb
B
3LL-R
^{3}H-Thymidine Incorporation (dpm)
2500
2000
1500
1000
500
0
***
*
*
***
FCS+L-Gln - + + + + + + +
T1317 (μM) - - 1 5 10 - - -
GW3965 (μM) - - - - - 1 5 10
C
WT
DMSO
T1317
Volume (mm^3)
1750
1500
1250
1000
750
500
250
0
**
7 8 9 10 11 12 13 14 15
Day
D
LXRα/β$^{-/-}$
DMSO
T1317
Volume (mm^3)
3500
3000
2500
2000
1500
1000
500
0
7 8 9 10 11 12 13 14 15
Day
E
Control
T1317
Tumor latency
150
100
50
0
0 50 100 150
Age (days)
F
Control
T1317
Mammary gland weight (g)
0.8
0.4
0
*
*
*
**
*
Gland 1
Gland 2-3
Gland 4-5
Gland 6
Gland 7-8
Gland 9-10
G
Total mammary gland weight (g)
2.5
2
1.5
1
0.5
0
***
Control
T1317

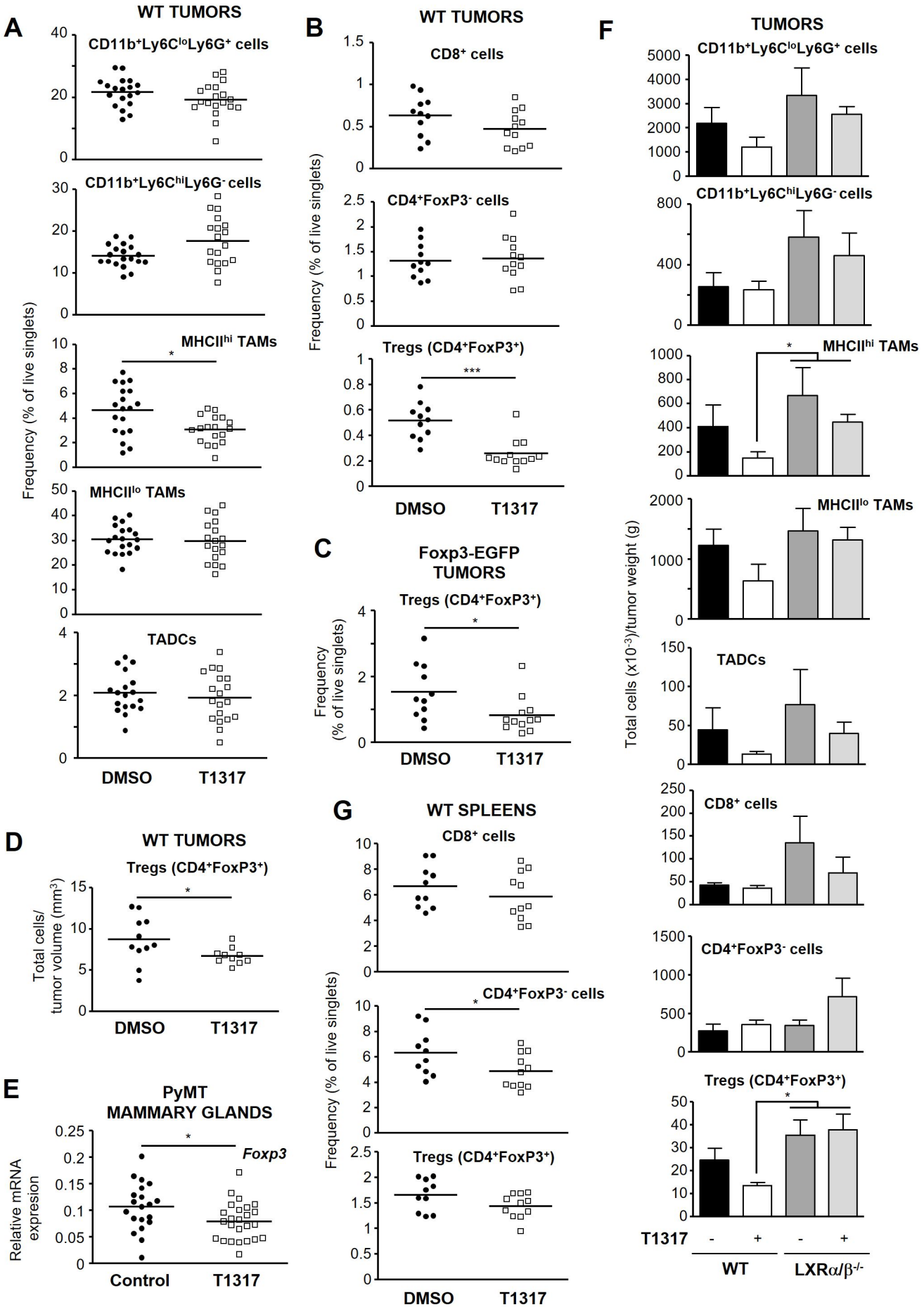

Carbó Leon et al. Fig. 2

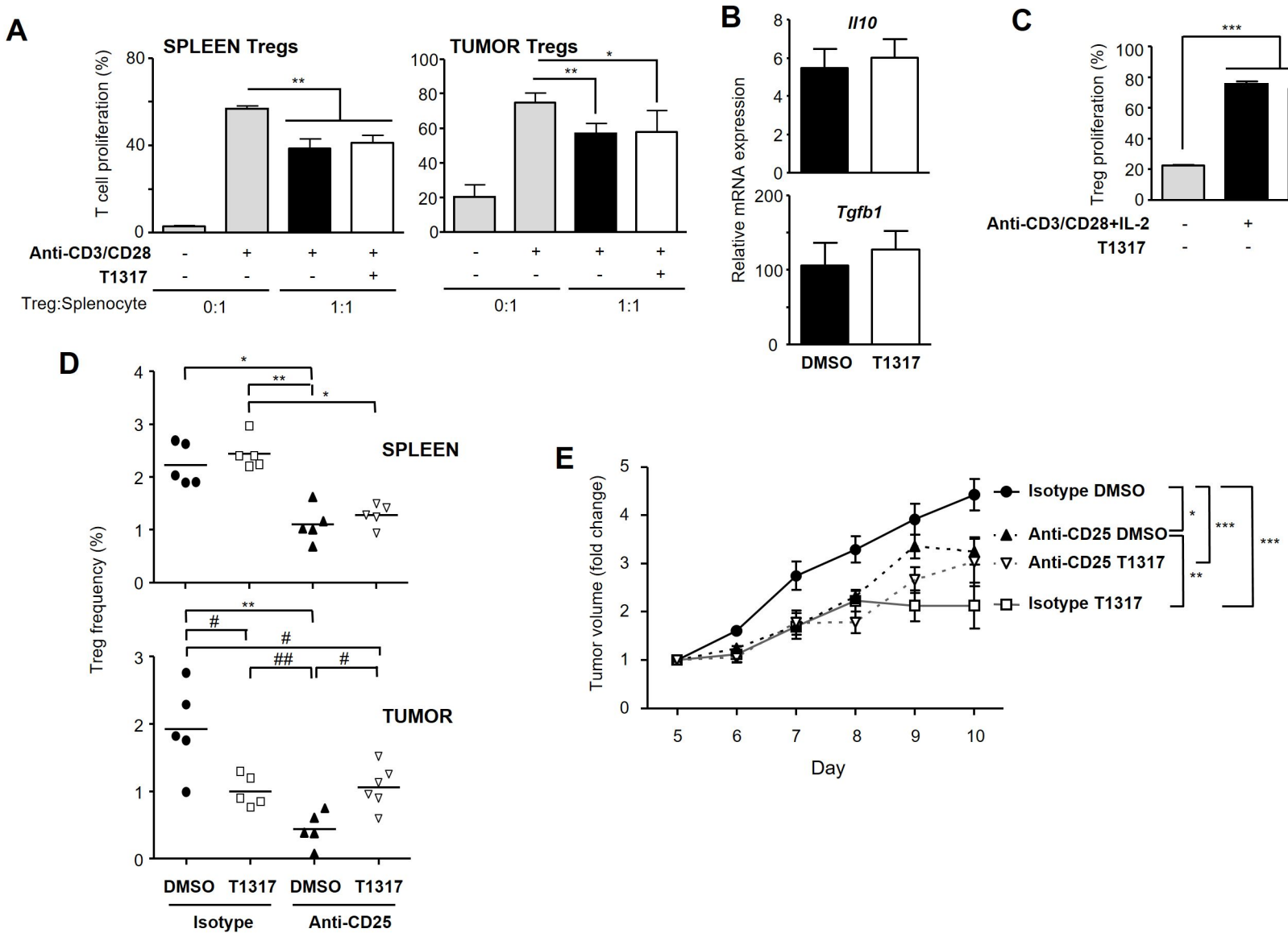
A
SPLEEN Tregs
TUMOR Tregs
T cell proliferation (%)
Anti-CD3/CD28
T1317
Treg:Splenocyte
0:1
1:1
B
Il10
Tgfb1
Relative mRNA expression
DMSO
T1317
C
Treg proliferation (%)
Anti-CD3/CD28+IL-2
T1317
D
SPLEEN
TUMOR
Treg frequency (%)
DMSO
T1317
Isotype
Anti-CD25
E
Tumor volume (fold change)
Day
Isotype DMSO
Anti-CD25 DMSO
Anti-CD25 T1317
Isotype T1317

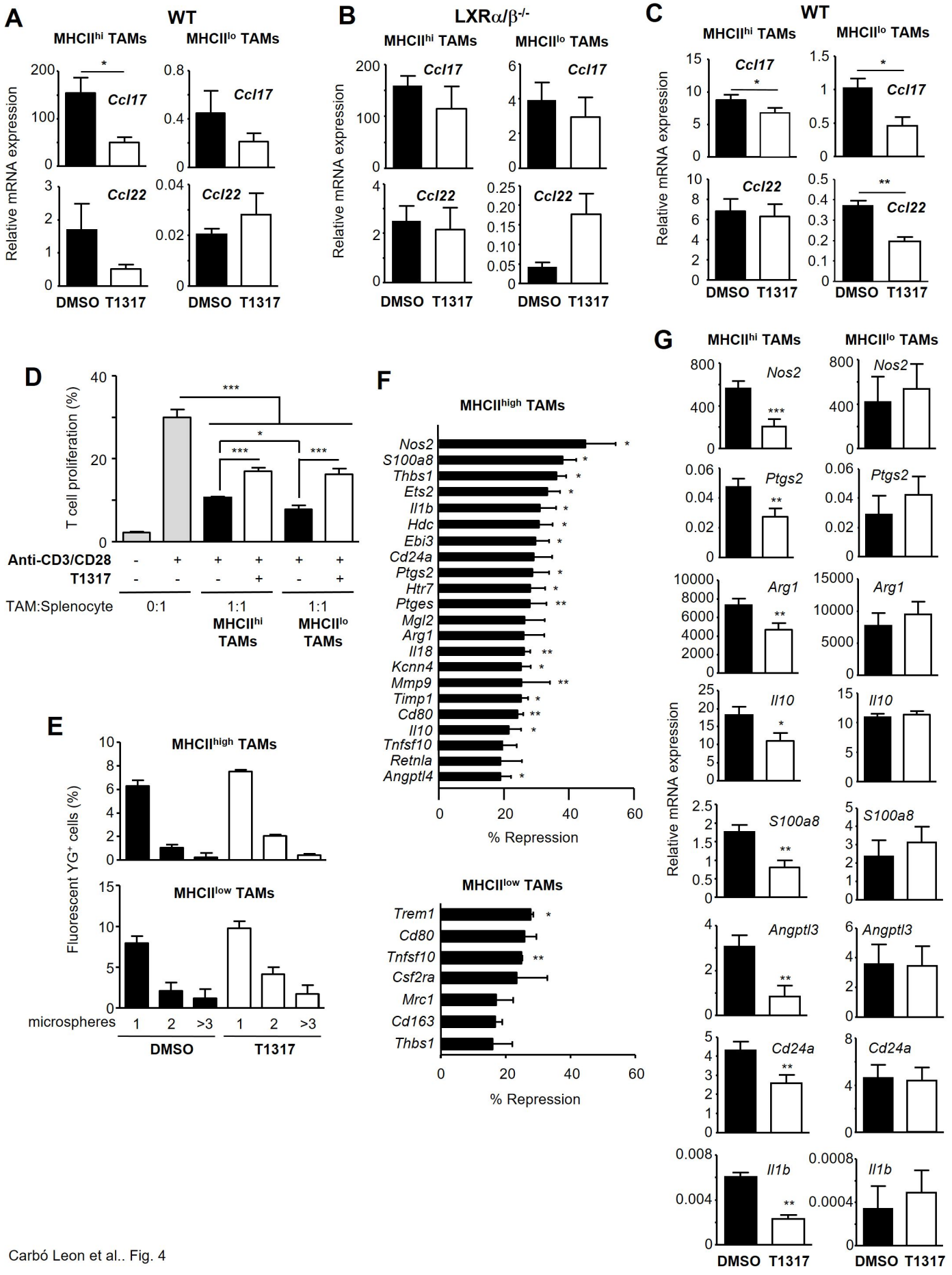

Carbó Leon et al.. Fig. 4

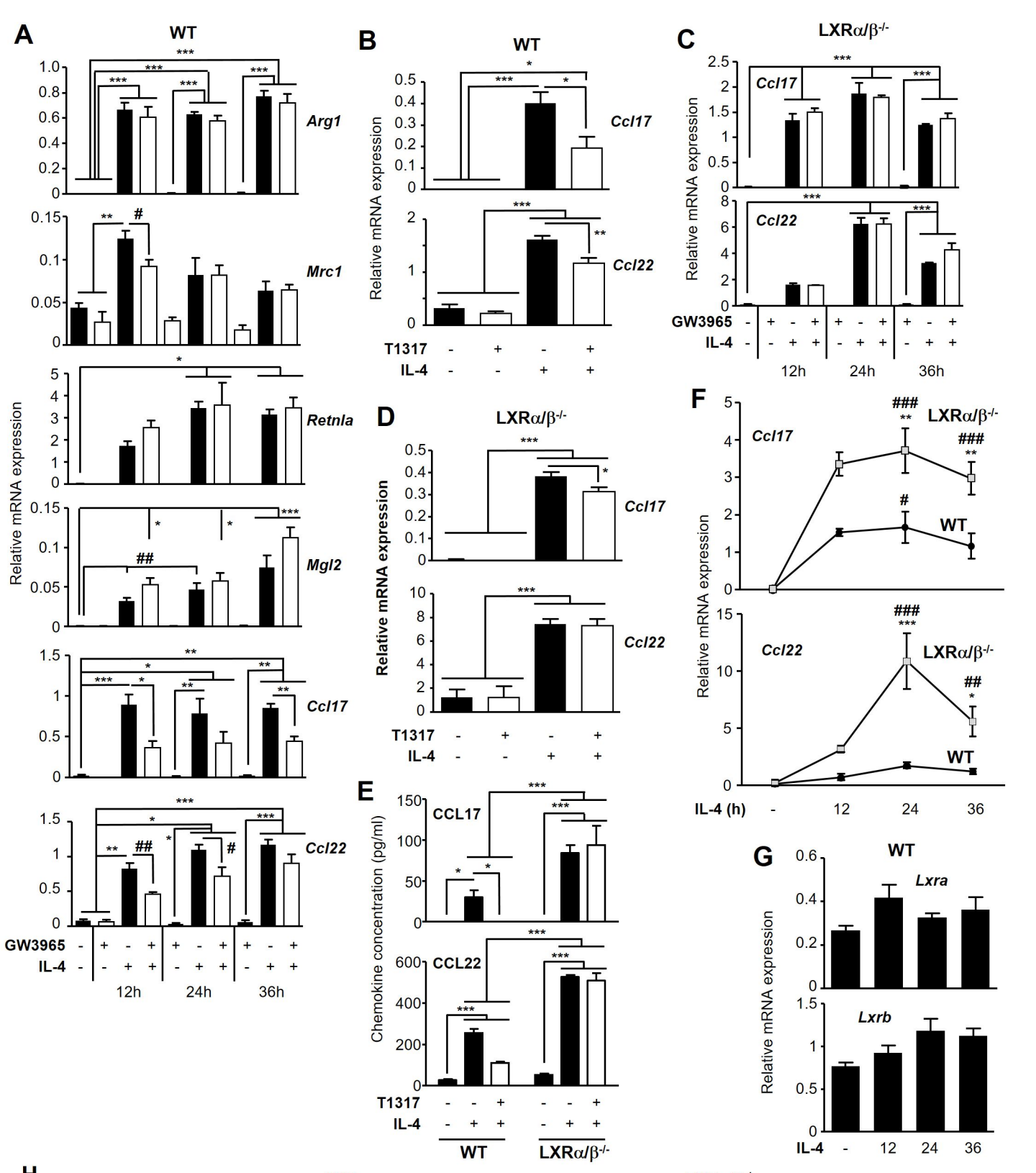

Carbó Leon et al. Fig. 5

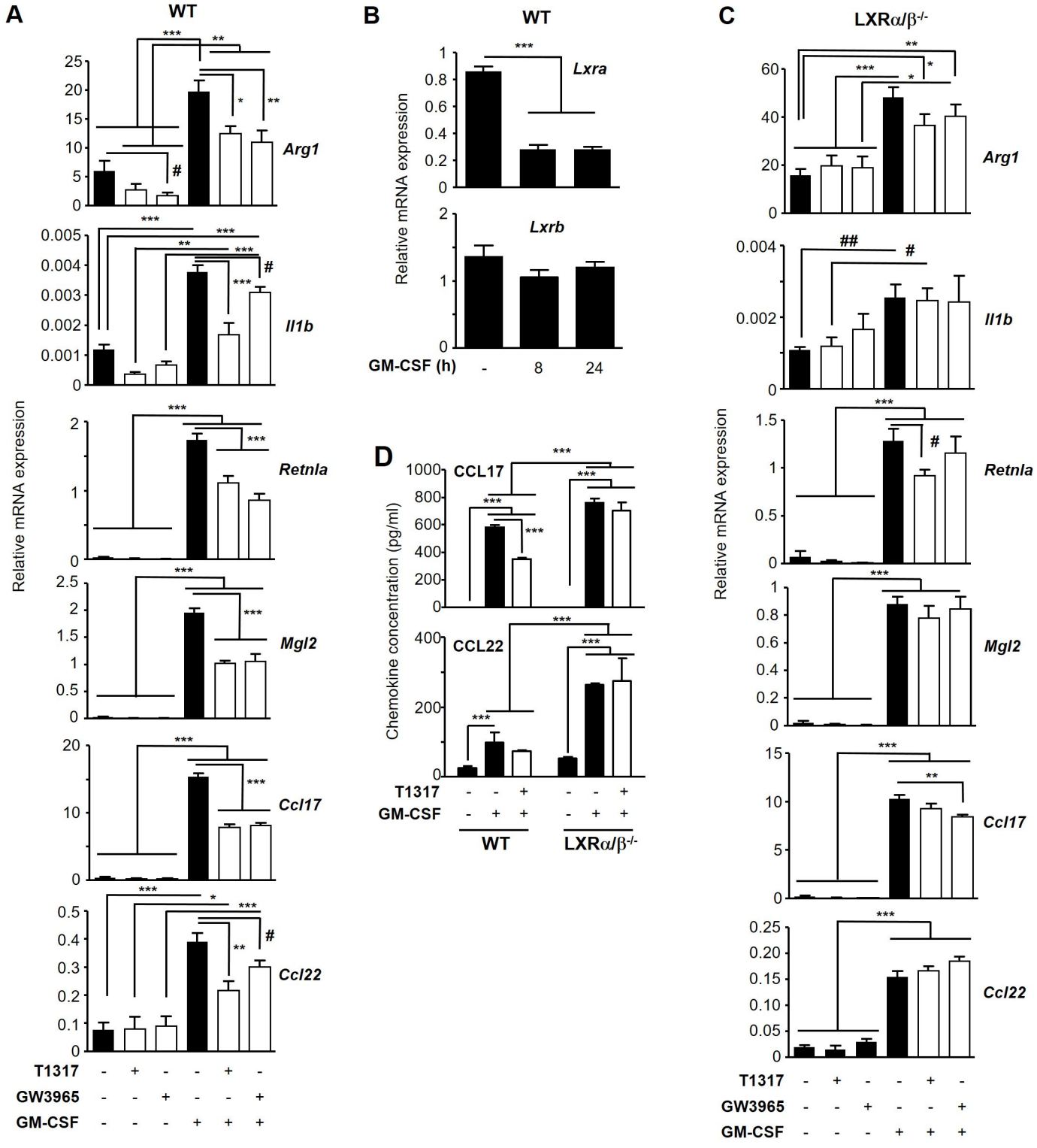
A
WT
Arg1
Il1b
Retnla
Mgl2
Ccl17
Ccl22
Relative mRNA expression
T1317
GW3965
GM-CSF
B
WT
Lxra
Lxrb
Relative mRNA expression
GM-CSF (h)
C
LXRα/β-/-
Arg1
Il1b
Retnla
Mgl2
Ccl17
Ccl22
Relative mRNA expression
T1317
GW3965
GM-CSF
D
CCL17
CCL22
Chemokine concentration (pg/ml)
T1317
GM-CSF
WT
LXRα/β-/-

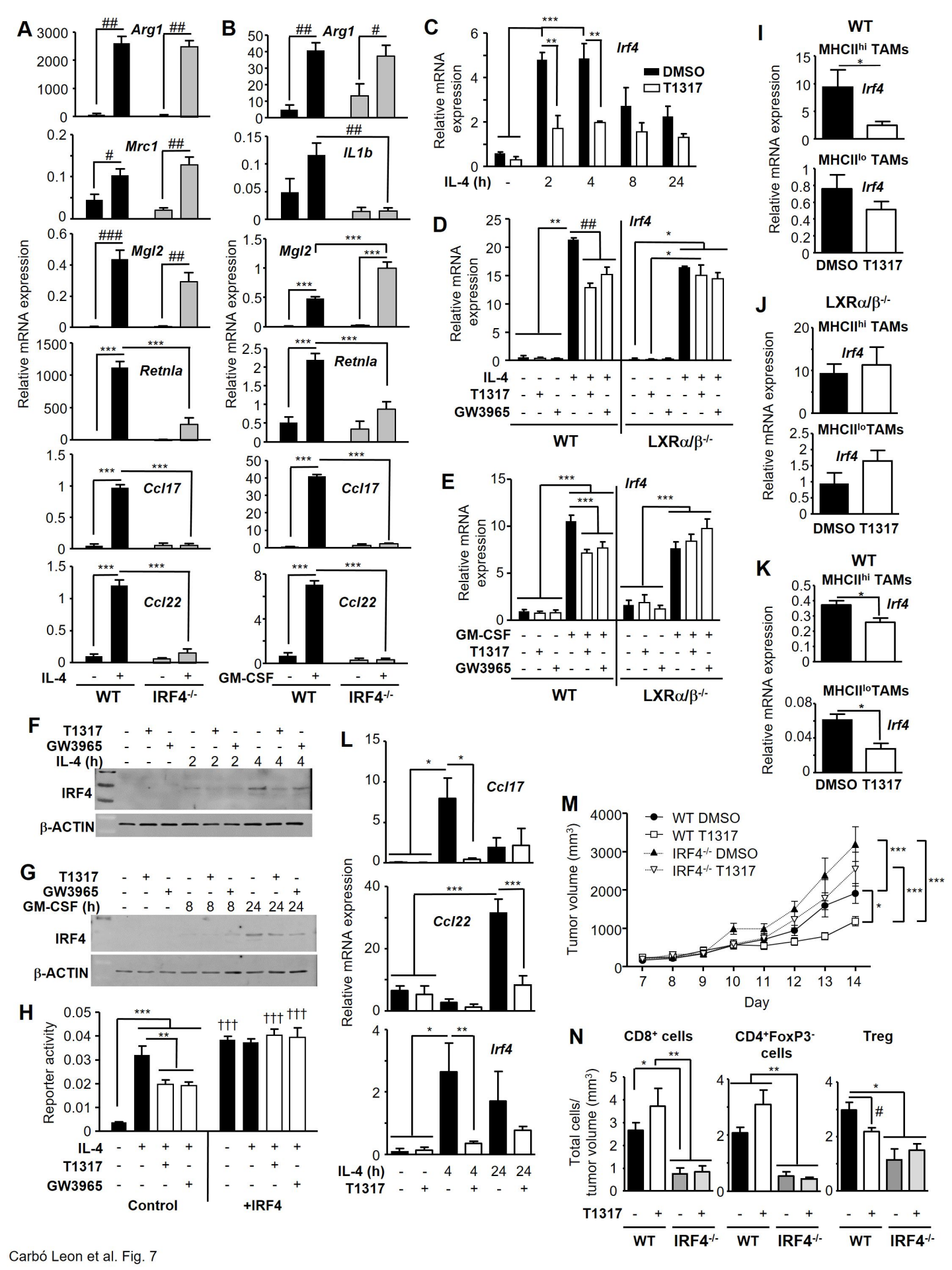

Carbó Leon et al. Fig. 7